UNCLASSIFIED

AD NUMBER
AD827961
LIMITATION CHANGES
TO: **Approved for public release; distribution is unlimited.**
FROM: **Distribution authorized to U.S. Gov't. agencies and their contractors; Critical Technology; DEC 1967. Other requests shall be referred to Air Force Rocket Propulsion Laboratory, Edwards AFB, CA. This document contains export-controlled technical data.**
AUTHORITY
AFRPL ltr, 27 Oct 1971

THIS PAGE IS UNCLASSIFIED

AFRPL-TR-67-319

AD827961

STRUCTURE AND REACTIVITY OF ENERGETIC CHEMICAL SPECIES

Larry Kevan
Marlin Harmony
Ralph Christoffersen
James Barnes

Department of Chemistry
University of Kansas
Lawrence, Kansas 66044

Annual Summary Report

December, 1967

This document is subject to special export controls and each transmittal to foreign governments or foreign nationals may be made only with prior approval of AFRPL (RPPR-STINFO), Edwards, California 93523.

Air Force Rocket Propulsion Laboratory
Research and Technology Division
Air Force Systems Command
Edwards Air Force Base, California

DDC
RECEIVED
MAR 6 1968
C

114

ACCESSION for
CFSTI WHITE SECTION
DDC BUFF SECTION
UNANNOUNCED
JUSTIFICATION
BY
DISTRIBUTION/AVAILABILITY CODES
DIST. AVAIL. and/or SPECIAL
2

When U.S. Government drawings, specifications, or other data are used for any purpose other than a definitely related Government procurement operation, the Government thereby incurs no responsibility nor any obligation whatsoever, and the fact that the Government may have formulated, furnished, or in any way supplied the said drawings, specifications, or other data, is not to be regarded by implication or otherwise, or in any manner licensing the holder or any other person or corporation, or conveying any rights or permission to manufacture, use, or sell any patented invention that may in any way be related thereto.

AFRPL-TR-67-319

This document is subject to special export controls and each transmittal to foreign governments or foreign nationals may be made only with prior approval of AFRPL (RPPR-STINFO), Edwards, California 93523.

STRUCTURE AND REACTIVITY OF ENERGETIC CHEMICAL SPECIES

Larry Kevan
Marlin Harmony
Ralph Christoffersen
James Barnes

FORWARD

This research was carried out under Contract No. F04611-67C-0032 with the University of Kansas, Lawrence, Kansas 66044, and was directed by Professor Larry Kevan in the Department of Chemistry. The Air Force program monitor was Dr. Lawrence P. Quinn (RPCL). This report covers research done between November 1, 1966, to October 31, 1967. This report was submitted in December, 1967.

This technical report has been reviewed and is approved.

W. H. EBELKE, Colonel, USAF
Chief, Propellant Division

ABSTRACT

Energetic chemical species have been investigated by both theoretical and experimental methods. The nature of the chemical bonding in H_3^+ has been studied by means of a natural spin orbital analysis of a previously calculated wavefunction. H_3^+ is shown to resemble closely its united atom analog, Li^+, and the Hartree-Fock energy of H_3^+ is estimated to be -1.301 hartrees. Also, electron density plots are presented in order to clarify the physical picture of the bonding in H_3^+, and suggestions are made as to how further calculations might proceed most efficiently. In the geminal theory of chemical bonding a new method has been developed for solving the coupled integro-differential equations for determination of the optical geminals for a system. Geminal theory has also been generalized to include odd electron systems. A microwave spectrometer employing Zeeman modulation and a flow cell has been built for studying transient paramagnetic species. Charge storage in γ-irradiated polymethylmethacrylate (PMMA) at room temperature has been studied by measuring thermoelectric currents. By using pure PMMA as well as PMMA doped with hole and electron traps it has been shown that added electron traps but not hole traps lead to charge stabilization. The thermoelectric currents appear to be due to hole mobility. The trapped charge in doped PMMA decays with an activation energy of 0.9 ev. Polyvinyl chloride stabilizes even larger amounts of charge than does doped PMMA.

TABLE OF CONTENTS

Scope of the Program 1

I. Theoretical Investigations

1. Introduction 2

2. Analysis of H_3^+

a. Purpose 4
b. The Wavefunction 5
c. The Natural Expansion 11
d. Truncated Expansions 14
e. A Symmetric Representation 19
f. Discussion 22
g. Conclusions 31

3. Geminal Theory 33

4. References 42

II. Microwave Spectroscopy of Transient Energetic Species

1. Introduction 44

2. Spectrometer Construction

a. The Complete Spectrometer 45
b. Sample Cell Design 45
c. Spectrometer Tests 49

3. Initial Studies

a. Free Radicals 53
b. Electronically Excited Species 54

4. References 57

III. Radiation-Induced Charge Storage in Organic Polymers

1. Introduction 58

2. Experimental

a. Sample Preparation 60
b. Current Measurement 61
c. Temperature Measurement 63
d. Temperature Gradients 67
e. Polymerization Techniques 70
f. Sample Irradiation 73

3. Results

a. Current Measurement 74
b. Dose Effects 77
c. Effect of Heating Rate 77
d. Zero Temperature Gradient 77
e. Successive Irradiations on the Same Sample 83
f. Variations of Sample Thickness 83
g. Decay Studies 89
h. Effect of Additives 94

4. Discussion

a. Model of Thermoelectric Current Generation 96
b. Stability of Trapped Charge 99
c. Sample Thickness Effects 100
d. Dose Saturation of Traps 100

5. References 102

LIST OF TABLES

Table I-I. Normalized Symmetry Orbitals 7

Table I-II. The Coefficient Matrix $\underline{C}$ of Equation 1 9

Table I-III. Overlap Matrix Δ over the Original Basis 10

Table I-IV. Natural Orbitals for H_3^+ 13

Table I-V. Summary of Occupation Number Data 17

Table I-VI. Summary of Hartree-Fock Calculations on Equilateral H_3^+ 17

Table II-I. New Zeeman Modulator Specifications 52

Table III-I. Effect of Absorbed Dose on Thermal Induced Charge Release in Lucite 78

Table III-II. Effect of Heating Rate on Thermal Induced Charge Release in Lucite 80

Table III-III. Successive Irradiations and Measurements of Thermoelectric Currents in Lucite 85

Table III-IV. Successive Irradiations and Measurements of Thermoelectric Currents in Polyvinyl Chloride 86

Table III-V. Decay of Trapped Charge Carriers in Lucite at Various Temperatures. 91

Table III-VI. Thermoelectric Currents from Synthesized Polymers . . . 95

LIST OF FIGURES

Figure I-1. A plot of the square of the first natural orbital along a line passing through one nucleus and the midpoint between the other two nuclei 24

Figure I-2. Electron density contours for the ground state H_3^+ as calculated from the first natural orbital 25

Figure I-3. Contour plots of constant values of Φ_r^2 (1) 27

Figure II-1. Spectrometer - block diagram 46

Figure II-2. Sample cell 47

Figure II-3. Prototype Zeeman modulator 48

Figure II-4. Dielectric rod transmission 50

Figure II-5. Discharge and mixing tube 55

Figure III-1. Teflon sample holder 62

Figure III-2. Circuit block diagram 64

Figure III-3. Noise filtering circuit 66

Figure III-4. Temperature gradient measurement on Lucite 1.0 cm thick 68

Figure III-5. Temperature gradient measurement on Lucite 0.1 cm thick 69

Figure III-6. Zero temperature gradient measurement 71

Figure III-7. Thermoelectric current plot for Lucite 75

Figure III-8. Thermoelectric current plot for PVC 76

Figure III-9. Thermal induced charge release vs absorbed dose 79

Figure III-10. Effect of heating rate on normalized total charge . . . 81

Figure III-11. Effect of heating rate on peak current 82

Figure III-12. Thermoelectric current plot for zero temperature gradient 84

Figure III-13. Current profiles for sample thicknesses from 1.0 cm to 0.17 cm 87

Figure III-14. Current profiles for sample thicknesses from 0.10 cm to 0.02 cm 88

Figure III-15. Net current vs sample thickness in Lucite 90

Figure III-16. Decay of thermoelectric currents in Lucite samples . . 92

Figure III-17. Arrhenius plot for thermoelectric current decay 93

STRUCTURE AND REACTIVITY OF ENERGETIC CHEMICAL SPECIES

SCOPE OF THE PROGRAM

The physics and chemistry of highly energetic chemical species such as ions, electronically and vibrationally excited molecules, and free radicals is still in its infancy. The greatest paucity of information concerns excited state species; their structure, reactivity, and metastability represent a newly developing, experimentally difficult, but potentially rewarding field of study. Theoretical techniques are just now arriving at the point at which they can provide accurate and detailed information on energetic species of chemical interest (e.g. H_3^+). Thus, theory is reaching the point where it can supplement and guide the experimental investigation of energetic species. The characteristics of energetic species of all types in the solid state is also an area of great importance and limited information.

The areas of study are vectored toward an enhanced understanding of the physical and chemical characteristics of highly energetic chemical species. A balanced experimental and theoretical study of both structure and reactivity of carefully selected species and systems utilizing a variety of techniques characterizes the general approach used. In this annual report progress is reported in the following areas: (a) nature of bonding in H_3^+, (b) geminal theory, (c) construction of a microwave spectrometer for studying transient energetic species, and (d) radiation-induced charge storage in organic polymers.

I. THEORETICAL INVESTIGATIONS

1. INTRODUCTION

The present theoretical aspect of the program is directed toward the theoretical elucidation of the structure, reactivity, and general nature of highly energetic species. In order to provide accurate and detailed information concerning compounds of potential interest as a rocket propellant as soon as possible, a multi-faceted program has been begun in which both specific compounds and general techniques are being studied simultaneously.

The work designed to elucidate the nature of particular species was centered on the H_3^+ molecule, both because it holds considerable interest as a reactive species, and because it can be used as a prototype for the description of the bonding in electron deficient systems.

The other area in which considerable progress has been made is in the development and implementation of a geminal theory of chemical bonding. This theory can be applied generally to give accurate results on systems of chemical interest, without losing all hope of interpreting the resulting wavefunction. Since geminal theory is still in its infancy, much fundamental analysis was necessary before computational algorithms could be developed, and much of this analysis was completed during this year. In particular, significant advances have been made in two separate aspects of pair theory. First of all, a new method has been developed for solving the coupled integro-differential equations that arise in the determination of the optimal geminals for a system. This method appears to hold

considerable promise toward significantly reducing the computational time that is necessary to determine the best set of geminals, without loss of accuracy. Secondly, it has been feasible to show that it is not only possible, but convenient, to include an odd electron into the general theory of geminals, so that the concept of geminals need not be restricted to systems with an even number of electrons.

As well as the aforementioned developments in the area of analysis, much of the work necessary to implement ab initio calculations using geminal theory has been carried out. Most of the computer programs to evaluate the one- and two-center integrals that arise in these calculations have now been written and tested on the GE-625 computer at the University of Kansas. This work involved a careful choice of the manner in which these programs were implemented. The result has been that the integral programs are presently very efficient and often run 3 to 4 times faster than other existing programs without loss of accuracy.

2. ANALYSIS OF H_3^+

a. Purpose

Although the small, reactive species, H_3^+, has been known to exist for a considerable length of time, the lack of experimental characterization of H_3^+ beyond confirmation that it exists has required that most knowledge of this molecule must come from theoretical considerations. To investigate the nature of H_3^+, the following analysis of an accurate wavefunction was carried out.

The use of a wavefunction which is derived from an arbitrarily chosen basis for interpretation of the nature of the bonding in two-electron systems often encounters severe difficulties. In a series of papers,[1-6] it has been emphasized that if one is to attempt to extract the real 'nature' of the bond, then one must make use of some invariant properties which are not solely a function of the arbitrary basis set chosen. There are various such invariant descriptions of a molecular system. The most commonly used one is the Hartree-Fock approximation,[7] or a close approximation thereto. This particular invariant description is an important one because energy is used as a criterion of excellence and because it can be shown that most one-electron properties are given correctly to second order by the exact Hartree-Fock function. Calculations now exist for an extensive series of molecules,[8] and informative and valuable correlations have been made using these results.

Unfortunately, the Hartree-Fock energy is far from the exact energy, usually farther than the entire binding energy of the molecule. Consequently, subleties in the molecular structure are imperfectly revealed by

studies of Hartree-Fock functions alone. Also, higher invariant approximations using minimum energy as a criterion of excellence rapidly become extraordinarily difficult to organize.[9]

As an alternative invariant description, the eigenfunctions and eigenvalues of the first order density matrix associated with a given trial function have been used. These eigenvalues are the occupation numbers of the natural orbitals, and even for quite approximate functions, have been found to be almost basis independent[10] in the systems examined thus far. Consequently, conclusions that can be drawn from the occupation numbers of natural orbital expansions appear to have a range of validity that is both esthetically pleasing and heuristically useful.

The results of a natural orbital analysis of the H_3^+ wavefunction reported by Christoffersen[11] are presented here. Since the energy of this wavefunction is close to that expected from the exact wavefunction, it is likely that it contains representative components of all important basis types. It appears that this analysis is not significantly different from one that would be obtained from the exact wavefunction, or from any other computed approximate wavefunction that has as low an energy expectation value as the wavefunction used.

b. The Wavefunction

We limit our consideration to the equilibrium position of the ground A_1' state of H_3^+. We have previously discussed in another connection natural orbitals and occupation numbers associated with some very crude functions for the linear conformation,[5] but as Christoffersen has

demonstrated, the equilateral conformation is by far the most stable. The wavefunction analyzed here is of the form

$$\Phi = \underline{\eta}^T (1)\, \underline{C}\, \underline{\eta}\, (2), \qquad (1)$$

in which $\underline{\eta}$ is a column vector of normalized (but not necessarily orthogonal) symmetry adapted orbitals, and $\underline{\eta}^T$ is the transpose of $\underline{\eta}$. In Table I-I we list the precise definitions of the individual η orbitals in terms of the original basis set of Slater type orbitals on each nucleus. Here a, A, α, $\alpha\pi$ are centered on the first vertex; b, B, β, or $\beta\pi$ on the second vertex, and c, C, γ, $\gamma\pi$ on the third vertex of the triangle. Lower case Roman letters refer to 1s orbitals:

$$(a,\ b,\ c) = (\zeta_1^3/\pi)^{\frac{1}{2}}\, e^{-\zeta_1 r}, \qquad (2)$$

capital Roman letters to 2s orbitals:

$$(A,\ B,\ C) = (\zeta_2^5/3\pi)^{\frac{1}{2}}\, r e^{-\zeta_2 r}, \qquad (3)$$

lower case Greek letters to 2p orbitals

$$(\alpha,\ \beta,\ \gamma) = \left(\frac{\zeta_3^5}{\pi}\right)^{\frac{1}{2}} r \cos\theta\, e^{-\zeta_3 r}. \qquad (4)$$

The p orbitals, α, β, γ, are directed from each nucleus towards the midpoint of the molecule. The p orbitals, $\alpha\pi$, $\beta\pi$, $\gamma\pi$ are directed perpendicular to the plane of the molecule. Christoffersen's calculations showed that p orbitals in the plane perpendicular to α, β, γ respectively were relatively unimportant, and these were omitted from the calculation analyzed here. The internuclear distance was taken at R = 1.6575 bohrs and the parameters chosen to be $\zeta_1 = 1.20$, $\zeta_2 = 1.175$, $\zeta_3 = 1.80$. This function gave a computed energy of -1.33264 hartrees.

Table I-1. Normalized symmetry orbitals. See text for definition of original basis.

Irreducible Representation	
a_1'	$\eta_1 = 0.391\ 133\ (a + b + c)$
a_1'	$\eta_2 = 0.354\ 868\ (A + B + C)$
a_1'	$\eta_3 = 0.476\ 514\ (\alpha + \beta + \gamma)$
e'	$\eta_4 = 1.103\ 552\ (a - c)$
e'	$\eta_5 = 1.682\ 978\ (A - C)$
e'	$\eta_6 = 0.807\ 925\ (\alpha - \gamma)$
e'	$\eta_7 = 0.637\ 136\ (2b - a - c)$
e'	$\eta_8 = 0.971\ 667\ (2B - A - C)$
e'	$\eta_9 = 0.466\ 456\ (2\beta - \alpha - \gamma)$
a_2''	$\eta_{10} = 0.421\ 669\ (\alpha\pi + \beta\pi + \gamma\pi)$
e''	$\eta_{11} = 0.942\ 691\ (\alpha\pi - \gamma\pi)$
e''	$\eta_{12} = 0.544\ 263\ (2\beta\pi - \alpha\pi - \gamma\pi)$

In Table I-II we exhibit the coefficient matrix $\underline{C}$. It should be noted that these coefficients are different from those reported by Christoffersen because we have now normalized the individual molecular orbitals composed of Slater-type basis orbitals. Since the original basis is chosen symmetry-adapted, the complete $\underline{C}$ matrix has many zeros from symmetry. Only the non-zero diagonal blocks are tabulated in Table I-II. Because of the doubly degenerate irreducible representation in the pertinent group D_{3h}, there is a duplication of blocks as indicated in the table. The 3-3, 6-6, and 9-9 configurations were omitted in the Christoffersen wavefunction.

It has already been indicated that the original basis is non-orthogonal. In Table I-III we tabulate the non-zero overlap integrals between the normalized basis functions η. One of the striking features of these numbers is the high values of many of the overlaps, especially that of Δ_{12} connecting the totally symmetric 1s and 2s functions. These values make questionable any attempts to make use of the coefficients of Table I-II in obtaining a handle on the real nature of the wavefunction. It is precisely for this reason that one strongly prefers to discuss the wavefunction in terms of its natural expansion.

Table I-II. The coefficient matrix $\underline{C}$ of equation 1.

Element	Value	Element	Value
c_{11}	1.385331	$c_{44} = c_{77}$	-0.123776
$c_{12} = c_{21}$	-0.285686	$c_{45} = c_{54} = c_{78} = c_{87}$	0.016589
$c_{13} = c_{31}$	0.092328	$c_{46} = c_{64} = c_{79} = c_{97}$	-0.022103
c_{22}	0.008291	$c_{55} = c_{88}$	-0.008559
$c_{23} = c_{32}$	0.001684	$c_{56} = c_{65} = c_{89} = c_{98}$	0.006762
c_{33}	0	$c_{66} = c_{99}$	0
$c_{10,10}$	-0.037462	$c_{11,11} = c_{12,12}$	-0.006999

All other elements are identically zero by symmetry.

Table I-III. **Overlap matrix Δ over the original basis.**

$\Delta_{12} = \Delta_{21} = 0.910431$	$\Delta_{45} = \Delta_{54} = \Delta_{78} = \Delta_{87} = 0.712956$
$\Delta_{13} = \Delta_{31} = 0.487879$	$\Delta_{46} = \Delta_{64} = \Delta_{79} = \Delta_{97} = -0.777956$
$\Delta_{23} = \Delta_{32} = 0.276857$	$\Delta_{56} = \Delta_{65} = \Delta_{89} = \Delta_{98} = -0.742063$

All diagonal elements of $\Delta = 1$. All other elements of Δ that are not explicitly given are zero.

c. The Natural Expansion

Since our basis is non-orthogonal, it is convenient to use the non-orthogonal formalism for obtaining the natural orbitals as outlined by Barnett, Linderberg and Shull.[12] The process is straightforward. Since we have a two electron problem, it is easier to diagonalize $\underline{C}\,\underline{\Delta}$ rather than $\underline{\chi}\,\underline{\Delta}$. The results are, of course, equivalent as shown by Löwdin and Shull.[13] We obtain natural orbitals of a_1', e', a_2'', and e'' symmetry. Since there was only one molecular orbital used of a_2'' type, and one degenerate pair of e'' type, the natural orbital occupation numbers of these are simply given by the squares of the corresponding coefficients $c_{10,10}$, $c_{11,11}$, and $c_{12,12}$ of Table II. On the other hand, 3×3 matrix products, $\underline{C}\,\underline{\Delta}$, must be diagonalized to obtain the natural orbitals of a_1' and e' symmetry. The results are listed in Table IV. The natural expansion of the wavefunction is then given by

$$\psi = \sum_i c_i \chi_i(1)\chi_i(2), \tag{5}$$

and the corresponding expansion of the first order density matrix by

$$\gamma = \sum_i n_i \chi_i(1)\chi_i(1') \tag{6}$$

with omission, of course, of the usual spin factors corresponding to a pure singlet function.

We consider first the occupation numbers. To place these in proper context we consider those of the united atom, Li^+,
and those of the singlet coupled separated atoms $H + H + H^+$, each an infinite distance from the others. For the latter, the correct wavefunction for the ground state is given by

$$\psi = \frac{1}{\sqrt{6}}\left\{a(1)b(2) + b(1)a(2) + a(1)c(2) + c(1)a(2) + b(1)c(2) + c(1)b(2)\right\},$$

omitting the usual singlet spin function. The occupation numbers for this case are 2/3 for the natural orbital $\frac{1}{\sqrt{3}}(a + b + c)$, and $\frac{1}{6}$ each for a degenerate pair

which might be, for example, $\frac{1}{\sqrt{2}}(a - b)$ and $\frac{1}{\sqrt{2}}(b - c)$ or any independent linear combinations of these. The symmetry of the first approximate natural orbital in this case is a_1', and the degenerate pair is e', just as is found for the actual H_3^+ function as analyzed in Table I-IV. On the other hand we note that the H_3^+ equilibrium state function has a much higher a_1' occupation number, and correspondingly lower values for e'.

The situation is more complex for the united atom. Natural orbitals in this case are of the usual types, s, p, d, etc. One needs to know the decomposition of these degenerate spherical harmonics into terms appropriate for the lower symmetry D_{3h}. Obviously s becomes a_1'. The three p levels split into $a_2'' + e'$; the five d levels split into $a_1' + e' + e''$; and so on.

One can make the very crude approximation that, even though the spherical degeneracies have been split, the occupation numbers remain equally divided among the components. This is expected to be a good approximation only at the united atom, but it allows a zeroth order comparison of occupation numbers. Shull[10] earlier has used a similar division of correlation energies in comparing He and H_2 with moderate success. Thus we assign one-third of the total p occupation in Li^+ to a_2'' and two-thirds to the two components of e'. We use occupation number data secured by Macias[14] from the 35 configuration function for Li^+ by Weiss.[15] The first six terms with total occupation number 0.999971 may thus be divided into $0.998121a_1'$, $0.000594a_2''$, $0.001223e'$, and $0.000033e''$.

The total a_1' occupation number $(n_1 + n_5 + n_{12})$ of 0.985680 for H_3^+ thus falls nicely into the sequence with the Li^+ a_1' total of 0.998121 and the separated atom total of 0.666667. The united atom character of H_3^+ is clearly evidenced. Correspondingly, the e' occupation total has climbed

Table I-IV. Natural Orbitals for H_3^+.

	Symmetry	c_i	n_i	χ_i
χ_1	a_1'	0.992404	0.984865	$1.191445\,\eta_1 - 0.275794\,\eta_2 + 0.093129\,\eta_3$
χ_2	e'	-0.079810	0.006370	$-1.215053\,\eta_4 + 0.081936\,\eta_5 - 0.220262\,\eta_6$
χ_3	e'	-0.079810	0.006370	$-1.215053\,\eta_7 + 0.081936\,\eta_8 - 0.220262\,\eta_9$
χ_4	a_2''	-0.037462	0.001403	η_{10}
χ_5	a_1'	-0.028547	0.000815	$0.978720\,\eta_1 - 1.566924\,\eta_2 + 0.573740\,\eta_3$
χ_6	e"	-0.006999	0.000049	η_{11}
χ_7	e"	-0.006999	0.000049	η_{12}
χ_8	e'	-0.006107	0.000037	$1.025436\,\eta_4 - 1.246616\,\eta_5 + 0.355811\,\eta_6$
χ_9	e'	-0.006107	0.000037	$1.025436\,\eta_7 - 1.246616\,\eta_8 + 0.355811\,\eta_9$
χ_{10}	e'	+0.001592	0.000002_5	$0.546234\,\eta_4 + 0.960382\,\eta_5 + 1.708073\,\eta_6$
χ_{11}	e'	+0.001592	0.000002_5	$0.546234\,\eta_7 + 0.960382\,\eta_8 + 1.708073\,\eta_9$
χ_{12}	a_1'	+0.000592	0.000000_4	$2.576951\,\eta_1 - 2.216009\,\eta_2 - 1.154724\,\eta_3$
			1.000000	

from the 0.001223 of the united atom to 0.012819 in H_3^+ towards 0.333333 for the separated atoms. On the other hand, the a_2'' occupation number of 0.000594 in the united atom increases to 0.001403 in H_3^+ and subsequently disappears in the separated atoms. The same kind of maximum is observed for the e" occupation.

The occupation number data are therefore not unexpectedly different from the united atom case, tending toward the separated atoms. The main changes are in the direction of transferring occupation from s type to p type terms associated with the transfer of in-out type of correlation to a more formally angular-type correlation which is more advantageous with separated nuclear centers. This data is summarized in Table I-V.

d. Truncated Expansions

Several calculations have been reported recently in which the Hartree-Fock energy of equilateral H_3^+ has been estimated. Using a Gaussian basis set of s- and p-type orbitals, Lester and Krauss[16] report a Hartree-Fock energy of -1.27778 hartrees at R = 1.68 bohrs. Preuss[17] used a larger Gaussian basis set of s-type orbitals and obtained a Hartree-Fock energy of -1.2988 hartrees at R = 1.62 bohrs. Also, in a one-center calculation using s, d, f, g and h orbitals, Joshi[18] reported a Hartree-Fock energy of -1.2863 hartrees at R = 1.2523 bohrs. Although a Hartree-Fock calculation was not explicitly carried out by the present authors, it is possible to obtain a reliable estimate of the Hartree-Fock energy from the analysis of the wavefunction reported here.

It has been shown that the energy calculated from a truncated natural expansion of one term (renormalized) is very close to the Hartree-Fock

energy, the error being of fourth order.[19,20] Since the wavefunction used in this analysis is quite flexible, it is expected that the energy of the first natural orbital will be quite close to the exact Hartree-Fock energy. The energy obtained using the first natural orbital was -1.2992 hartrees at R = 1.6575 bohrs, and possesses an overlap with the final wavefunction of 0.9024038. Since the optimum SCF energy has been observed to occur at a slightly shorter distance than the observed equilibrium distance[3] in H_2, it might be expected that the value of -1.2992 hartrees might be lowered slightly by performing a calculation at the equilibrium distance observed in other SCF calculations[17,18] (R = 1.62 bohrs). However, it has also been observed that the potential surface is quite flat with respect to variation of R.[17] On this basis it was anticipated that the energy improvement obtained by such a calculation would be negligible, and it was not carried out.

The proximity of the present value of -1.2992 hartrees to the Hartree-Fock energy can be further elucidated in the following manner. For a similar two-electron system, HeH^+, S. Peyerimhoff found[21] that a basis set consisting of only six basis orbitals ($\sigma 1s_{He}$, $\sigma 2s_{He}$, $\sigma 2s'_{He}$, $\sigma 2p_{He}$, $\sigma 1s_H$, $\sigma 2p_H$) with optimized orbital exponents gives a Hartree-Fock energy within approximately 0.0008 hartrees of the true Hartree-Fock energy. Since the basis set of 1s, 2s, 2pσ, 2pπ orbitals employed for the calculations[11] on H_3^+ is very similar to that used by Peyerimhoff, including optimization of orbital exponents, it seems likely that the error in the Hartree-Fock energy of H_3^+ is probably only slightly larger than the error in the six basis orbital calculation of Peyerimhoff. The error due to the additional nucleus in

H_3^+ is not easily estimable, but if we allow 0.001 hartrees as the error estimate of this complication, we may combine this with the error estimate of 0.0008 hartrees associated with a similar basis set, and estimate the Hartree-Fock energy of H_3^+ to be approximately -1.301 hartrees. A summary of recent Hartree-Fock calculations is given in Table I-VI.

Each of the two electron species that is closely related to H_3^+ has a correlation energy which is approximately constant, with H_2, HeH^+, and Li^+ having the values 0.041 hartrees,[22] 0.042 hartrees[21] and 0.043 hartrees,[23] respectively. Since the orbital shapes differ greatly in these three species, it appears that the shape of an orbital does not play a significant role in determining the correlation energy of two-electron systems. It has also been shown[24] that the correlation energy for two-electron atoms remains essentially constant at 0.040-0.045 hartrees, regardless of the nuclear charge. Since the size of a given orbital is determined largely by the nuclear charge, the constancy of the correlation energy for isoelectronic two electron atoms implies that the size of the orbital is also an unimportant factor in determining the correlation energy. Since the orbitals of H_3^+ differ from the orbitals in the isoelectronic analogs mostly in size and shape, it is likely that the correlation energy for H_3^+ will also lie within the range 0.040-0.045 hartrees. If we take 0.042 hartrees as the estimated correlation energy for H_3^+, then we obtain a value of -1.343 hartrees as the estimated true total energy of H_3^+.

It is interesting to note that this estimate of the total energy is considerably above the value of -1.357 hartrees reported by H. Conroy.[25] Since the method used by Conroy is not constrained by the variation theorem, it is possible that the extrapolated results may lie either above or below

Table I-V. Summary of Occupation Number Data

	a_1'	e'	a_2''	e''
Li^+	0.998121	0.001223	0.000594	0.000033
H_3^+	0.985680	0.012819	0.001403	0.000098
$2H + H^+$	0.666667	0.333333	0.000000	0.000000

Table I-VI. Summary of Hartree-Fock Calculations on Equilateral H_3^+

Reference	Method	R_{HH}(bohrs)	E_{HF} (hartrees)
W. A. Lester and M. Krauss[a]	Gaussian orbitals	1.68	-1.27778
B. D. Joshi[b]	One-center expansion, Slater-type orbitals	1.623	-1.2863
H. Preuss[c]	Gaussian orbitals	1.62	-1.2988
M. E. Schwartz[d]	Gaussian orbitals	1.6505	-1.2999
Present Results	First natural orbital	1.6575	-1.2992
Estimated "true" Hartree-Fock energy	-	-	-1.301

[a] Reference 16.

[b] Reference 18.

[c] Reference 17.

[d] Private communication.

the true energy. In a similar comparison of calculations on HeH^+, Michels[26] pointed out that the extrapolated energy obtained by Conroy appeared to be too low, since the extrapolated value fell below that of a generalized 64-term James-Coolidge type wavefunction used by Wolniewicz.[27] Although the wavefunction employed by Christoffersen for H_3^+ (12 configurations) is not as flexible as the one used by Wolniewicz[27] for HeH^+, it is probably as flexible as the 11 configuration wavefunction for HeH^+ used by Anex,[6] which differs by only 0.0037 hartrees in total energy from the Wolniewicz wavefunction. Furthermore, the use of a Slater-type basis set for H_2 by McClean, Weiss and Yoshimine[28] similar to that used for H_3^+ resulted in an error of 0.007 hartrees in the total energy. Consequently, it appears that the error of ~0.01 hartrees to be added to the total energy of -1.33264 hartrees from the H_3^+ calculation[11] as implied above is a reasonable estimate, and that the value of -1.357 hartrees reported by Conroy may be too low.

Since the natural orbital expansion of rank two can always be expressed in "u,v" form which has the physical intuitional simplicity of the Heitler-London approach, it is also of interest to find the energy of the natural expansion of rank two for the present wavefunction. In this case, the "two term" expansion is actually composed of three terms, necessitated by the degeneracy of χ_2 and χ_3. The energy obtained for this truncated (and renormalized) function was -1.326 hartrees at R = 1.6575 bohrs. The overlap of this function with the complete wavefunction is 0.9988089 at the equilibrium distance.

e. A Symmetric Representation

Visual interpretation of three-fold systems is very much hindered by the necessary presence of doubly degenerate representations, e' and e". Although these two representations as a whole have three-fold density, they do not provide an easy way to discuss three equivalent relatively localized parts which may be associated with (in this case) H-H "bonds". For example, the real representations, η_4 and η_7 in Table I-I do not treat the three atoms equivalently in each orbital. One can avoid this by going to an imaginary representation with, for example,

$$e'_+ = \left[\frac{1}{3(1-S)}\right]^{\frac{1}{2}} (a + wb + w^*c) \tag{7}$$

and

$$e'_- = \left[\frac{1}{3(1-S)}\right]^{\frac{1}{2}} (a + w^*b + wc) \tag{8}$$

each of which clearly has 3-fold symmetry. But then there is still no convenient localized formulation, for the orbitals χ_1, e'_+ and e'_- are not three-fold equivalent.

We suggest that an attractive alternative formulation can be obtained by choosing one localized representative of the e' pair, and generating two equivalent (but non-orthogonal) representatives by successive application of the C_3^+ operation. Thus consider

$$\psi = \lambda_1^2 \chi_1(1)\chi_1(2) - \lambda_2^2 [\chi_2(1)\chi_2(2) + \chi_3(1)\chi_3(2)], \tag{9}$$

where χ_2, χ_3 form the degenerate pair. Suppose χ_2 to be as localized as possible in one "bond". Then we choose as bases for the e' representation:

$$\begin{aligned} \chi_r &\equiv \chi_2 \\ \chi_s &= C_3^+ \chi_2 = (-\sqrt{3}\,\chi_3 - \chi_2)/2 \\ \chi_t &= C_3^- \chi_2 = (+\sqrt{3}\,\chi_3 - \chi_2)/2. \end{aligned} \tag{10}$$

We note that these orbitals are normalized but are not orthogonal. Their mutual overlaps are precisely -1/2.

In this representation we can now write

$$\psi = \lambda_1^2 \chi_1(1)\chi_1(2) - \frac{2}{3}\lambda_2^2 [\chi_r(1)\chi_r(2) + \chi_s(1)\chi_s(2) + \chi_t(1)\chi_t(2)],$$

and hence

$$\begin{aligned} \psi = &\frac{1}{3}[\lambda_1^2 \chi_1(1)\chi_1(2) - 2\lambda_2^2 \chi_r(1)\chi_r(2)] \\ &+ \frac{1}{3}[\lambda_1^2 \chi_1(1)\chi_1(2) - 2\lambda_2^2 \chi_s(1)\chi_s(2)] \\ &+ \frac{1}{3}[\lambda_1^2 \chi_1(1)\chi_1(2) - 2\lambda_2^2 \chi_t(1)\chi_t(2)], \end{aligned} \tag{11}$$

in which ψ has now been divided into three separate localized "sum of squares" form. These may individually be expressed in "u, v" form so that

$$\Phi = \{ [u_r(1) v_r(2) + v_r(1) u_r(2)] + [u_s(1) v_s(2) + v_s(1) u_s(2)] + [u_t(1) v_t(2) + v_t(1) u_t(2)] \} / 3, \tag{12}$$

where

$$u_r = \lambda_1 \chi_1 + \sqrt{2}\, \lambda_2 \chi_r$$
$$v_r = \lambda_1 \chi_1 - \sqrt{2}\, \lambda_2 \chi_r, \tag{13}$$

and similarly for the other u's and v's. At this level of approximation, H_3^+ can be written as the sum of three equivalent (but geometrically displaced) two-electron "bonds" of Heitler-London type.

It is crucial to choose χ_2 to be as "bond-like" as possible, i. e., most localized in bond rather than on an atom. This choice is intuitively clearly $(b - c) / \sqrt{2(1 - S)}$, which has no contribution from atom a at all. Truncating the Christoffersen wavefunction to the first three natural orbitals, and making this phase choice for χ_2 we have finally

$$u_r = 0.996792\, \chi_1 + 0.399764\, \chi_r$$
$$v_r = 0.996792\, \chi_1 - 0.399764\, \chi_r. \tag{14}$$

Inserting the forms for χ_1 and $\chi_r = \chi_2$ from Table IV, collecting coefficients, we arrive at the following representatives for u and v in the original basis:

$$\begin{aligned} u_r = & -0.071515 \cdot a + 0.464518 \cdot b + 1.000551 \cdot c \\ & -0.0424304 \cdot A - 0.0975565 \cdot B - 0.152683 \cdot C \\ & -0.0269052 \cdot \alpha + 0.0442349 \cdot \beta + 0.115375 \cdot \gamma, \end{aligned} \tag{15}$$

and

$$v_r = 1.000551 \cdot a + 0.464518 \cdot b - 0.071515 \cdot c$$
$$-0.152683 \cdot A - 0.0975565 \cdot B - 0.0424304 \cdot C \qquad (16)$$
$$+0.115375 \cdot \alpha + 0.0442349 \cdot \beta - 0.0269052 \cdot \gamma,$$

where u_r and v_r have not been normalized. Further visualization of localized representatives will be given in the following section.

f. Discussion

We have already seen that one of the benefits of a natural spin orbital analysis is an estimate of the Hartree-Fock energy of H_3^+. Several other dividends can be gained via this analysis, not the least of which is an indication of the importance of various terms in the configuration interaction expansion.

One interesting point to note concerning the occupation numbers and their associated symmetry types given in Table I-IV is that, with the exception of the a_1' representation, a natural orbital of each symmetry type appears once before any repetition occurs. This suggests that, for further configuration interaction or similar studies of H_3^+, and perhaps for other molecules with similar bonding characteristics, the most rapid convergence of a many configuration wavefunction will be obtained by first including molecular orbitals of all of the various symmetry types, rather than adding further terms of the same symmetry. In cases where only limited size basis sets can be employed, this principle should be of particular importance. In the case of H_3^+, the molecular orbitals that were used represent all of the possible symmetry types except a_1''. The way in which a molecular orbital of this type can be formed is by using

Slater-type orbitals of the d_{xy} type, where the x, y, z axes on a given nucleus are chosen with the x, z plane as the plane of the molecule, and the z-axis pointing toward the center of the molecule. These orbitals give rise to two possible molecular orbitals, belonging to the a_1'' and e'' irreducible representations of D_{3h}. Table I-IV suggests that the use of an a_1'' molecular orbital in an acceptable configuration would result in a natural orbital with an occupation number greater than 0.000037, and probably between .000049 and 0.000815.

One of the intriguing aspects of H_3^+ left unanswered in the previous work[11] was that of the bonding arrangement in H_3^+. In order to elucidate the bonding in H_3^+, an electron density plot was made along a line from one nucleus through the center of the molecule, as well as a contour map of χ^2, and these plots are given as Figures I-1 and I-2. As can be seen, the electronic charge at the center of the molecule is greater than that at the midpoint of a line between nuclei.[29] Specifically, the value of χ^2 at the center of the molecule is 0.1157, and the value of χ^2 at the midpoint between two nuclei is 0.1036. Thus, if we subtract off the large electron density at each nucleus, there would remain a build-up of density at the center of the molecule. This observation affords further evidence to justify the earlier speculation that one appropriate description of the bonding arrangement in H_3^+ would be a set of three "bonds" pointing from the nuclei to the center of the molecule, rather than by bonds along the lines between the nuclei.[11]

Alternatively, the localized representatives of (u, v) form that were introduced in the previous section can be used to describe the bonding if

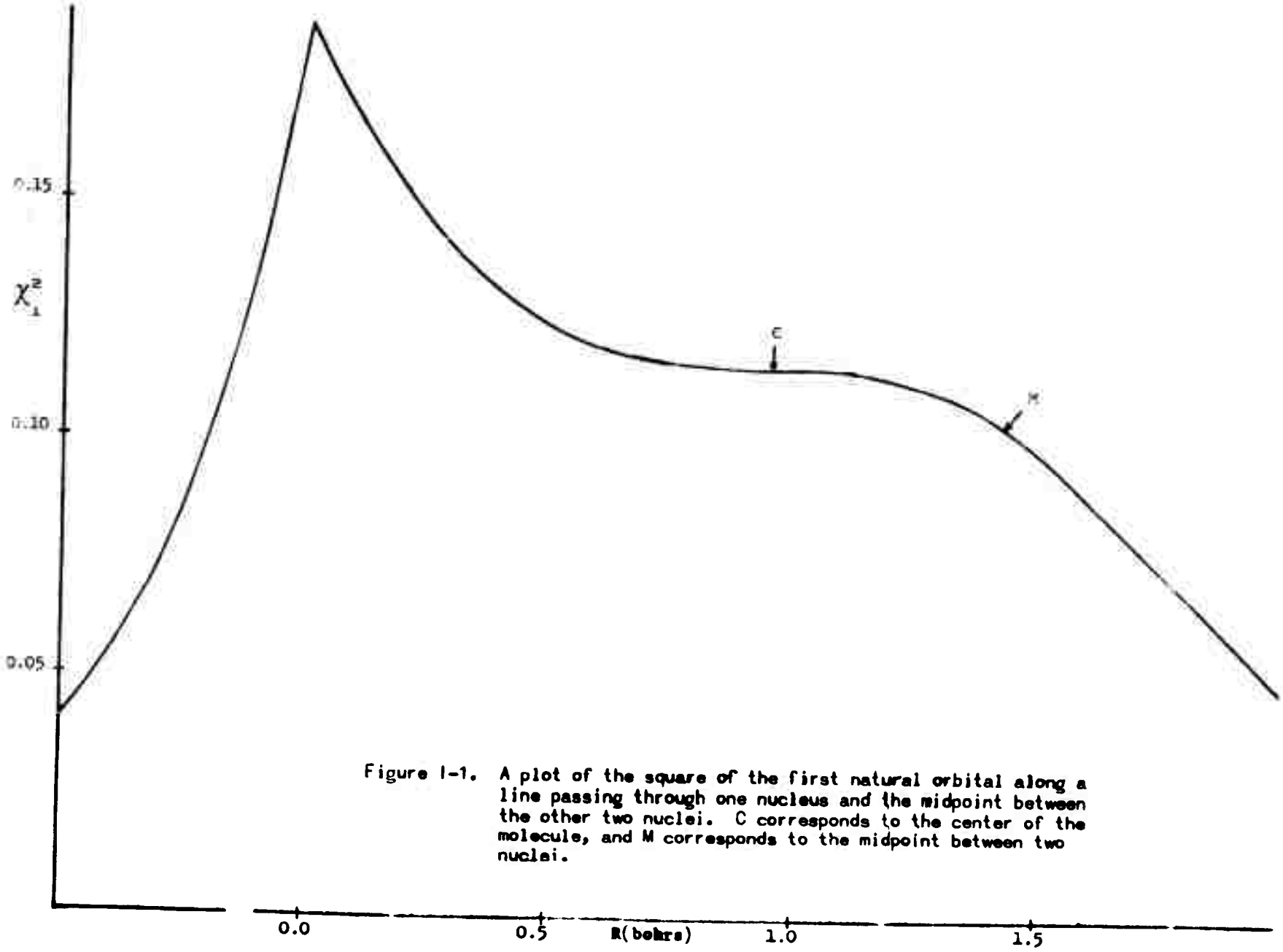

Figure I-1. A plot of the square of the first natural orbital along a line passing through one nucleus and the midpoint between the other two nuclei. C corresponds to the center of the molecule, and M corresponds to the midpoint between two nuclei.

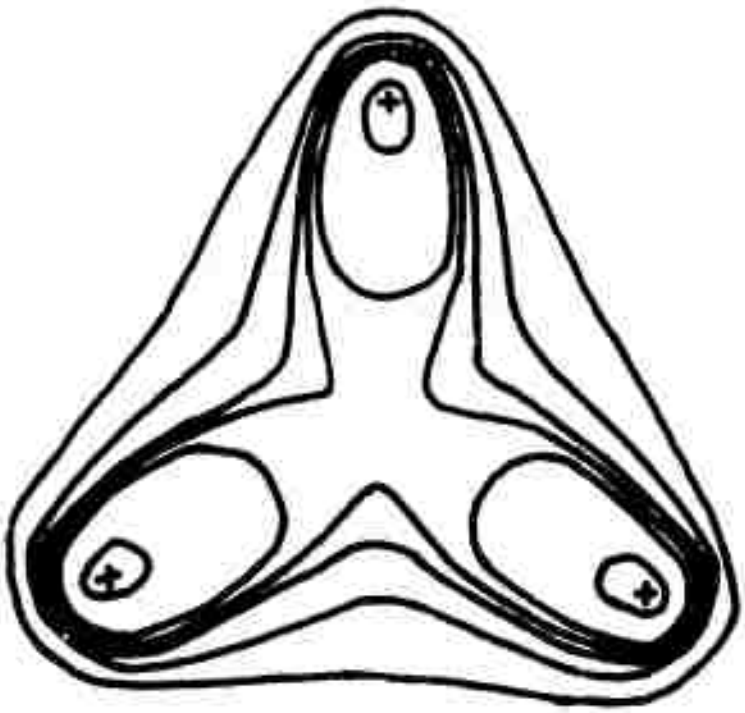

Figure 1-2. Electron density contours for the ground state H_3^+ as calculated from the first natural orbital. Proceeding outward from any given nucleus, the contours correspond to the following values of χ_1^2: 0.160, 0.120, 0.115, 0.110, 0.100, and 0.080.

three equivalent bonds are desired. However, these "bonds" are considerably "bent", which can be seen in the following manner.

From equation (11), we write one of the three equivalent "bonds" as

$$\Phi_r(1,2) = N\,[\,u_r(1)\,v_r(2) + v_r(1)\,u_r(2)\,]\,. \qquad (17)$$

We can obtain a visual representation of Φ_r by forming the square of Φ_r and integrating over the coordinates of electron two to give

$$\Phi_r^2(1) = 0.284716\,[\,u_r^2(1) + v_r^2(1)\,] + 0.411635\cdot u_r(1)\,v_r(1), \qquad (18)$$

which gives a representation of the electron density of electron one, averaged over all positions of electron two. Contour plots of constant $\Phi_r^2(1)$ are given in Figure I-3, which clearly show the "bent" character of the bond representation.

Since H_3^+ can be considered to be the triatomic analog of the homonuclear diatomic molecule (H_2), it is interesting to see if the concepts of fractional natural alternant character and fractional natural ionic character that have been developed for homonuclear diatomics[1] can be carried over to the polyatomic system. For the diatomic systems, the fractional natural alternant character (λ_A^2) and the fractional natural ionic character (λ_+^2) are defined by

$$\lambda_A = [\,(n_1)^{\frac{1}{2}} + (n_2)^{\frac{1}{2}}\,]/\sqrt{2},$$

$$\lambda_+ = [\,(n_1)^{\frac{1}{2}} - (n_2)^{\frac{1}{2}}\,]/\sqrt{2}, \qquad (19)$$

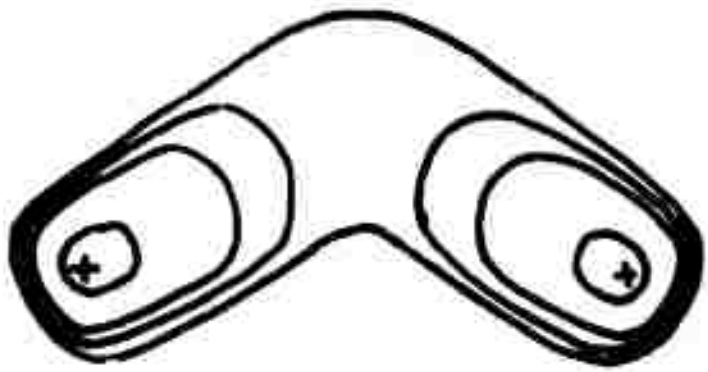

Figure 1-3. Contour plots of constant values of $\Phi_r^2(1)$. (See equation (18) in the text.) The contours correspond to the following values of $\Phi_r^2(1)$: 0.165, 0.125, 0.115 and 0.107.

where n_1 and n_2 are the occupation numbers (renormalized) of the two configuration natural expansion of the wavefunction.

In the case of H_3^+, we have already seen that it is possible to express the molecule in terms of three equivalent "bonds". However, in order to obtain the amount of alternant and ionic character for these "bonds", it is necessary to transform the expression describing these "bonds" into natural orbital form. This can easily be done by constructing two new orthonormal orbitals, ξ_+ and ξ_-, from u and v by

$$\xi_+ = (u+v)/N_+$$

$$\xi_- = (u-v)/N_- , \tag{20}$$

where

$$N_\pm = \int u^2 dV + \int v^2 dV \pm 2 \int uv dV. \tag{21}$$

The expression for the "bonds" in equation (17) can then be written in natural orbital form as

$$\Phi_r(1,2) = N\left[\left(\frac{N_+}{2}\right)\xi_+ - \left(\frac{N_-}{2}\right)\cdot\xi_-\right], \tag{22}$$

or

$$\Phi_r(1,2) = 0.987311\cdot\xi_+ - 0.158800\cdot\xi_-. \tag{23}$$

Using this data in equation (19), we see that the fractional natural alternant character and fractional natural ionic character of each of the three "bonds" in H_3^+ is given by

$$\lambda_A^2 = 0.6568$$

$$\lambda_+^2 = 0.3432. \tag{24}$$

For comparison purposes, the same calculation[3] at the equilibrium distance (R = 1.4 bohrs) for H_2 results in $\lambda_+^2 = 0.394$

and $\lambda_A^2 = 0.606$, and for R = 1.3 bohrs in He_2^{++}, the calculation results[4] in $\lambda_+^2 = 0.3583$ and $\lambda_A^2 = 0.6417$. Thus we may conclude that the degree of natural ionic character of each of the "bonds" in H_3^+ and the bonds in H_2 and He_2^{++} is very similar, with H_3^+ falling just below He_2^{++} and H_2.

The observation concerning the nature of the electron distribution in H_3^+ is in disagreement with the results of Preuss.[17] In one set of calculations using 17 1s-type Gaussian orbitals, he found that the Hartree-Fock energy of H_3^+ as calculated with two Gaussians placed in the center of the molecule was almost the same as the energy obtained when the two functions were absent from the center. This resulted in the conclusion that there was only a small electron density at the center of the molecule. Unfortunately, conclusions drawn from an examination of coefficients of terms involving a non-orthogonal basis set are vulnerable to criticism.

The basis functions of Preuss are far from being orthonormal, with the overlap of the various functions on the nuclei with the two orbitals in the center varying from 0.21584 to 0.90869. Consequently, we would like to suggest that an alternative conclusion is possible from the same data.

A calculation of the electron density in the center of the molecule using the Preuss wavefunction gives $\psi^2 = 0.118$, compared to $\chi^2 = 0.116$ from this work. Similarly, a point midway between two nuclei gives $\psi^2 = 0.102$, compared to $\chi^2 = 0.104$ from this work. Therefore, although it is not apparent from an examination of the coefficients in the non-orthogonal wavefunction, the Preuss wavefunction provides essentially the same description of the electron density in H_3^+ as our χ_1. Furthermore, the correct form for the electron density had already been established before the addition of the Gaussians in the center of the molecule, for a calculation

of ψ^2, omitting φ_{16} and φ_{17}, also results in a larger density in the center of the molecule, compared to the density at the midpoint between the nuclei. Thus, the addition of Gaussians in the center had little effect, but only corrected small defects in the electron distribution provided by the Gaussians already present. This should not be interpreted as a lack of electron density at the center of the molecule.

The above discussion might be construed to imply that a one-center calculation on H_3^+ would be rather effective. This approach has met with only very limited success[18,30] because, although there is a build up of electron density in the center relative to the midpoint of a line between nuclei, the electron density at either of these points is still far lower than at any of the nuclei. Therefore, the usual problem associated with one center calculation is also present in H_3^+, i.e., how does one build up charge density at off-center nuclei? Thus, it is not expected that significantly better results will be obtained for H_3^+ using a one-center approach than for any other molecular system with off-center nuclei.

As this work indicates, a great deal of insight has been gained into the nature of H_3^+, but the intriguing question of its lack of experimental characterization still remains. For example, its extremely high binding energy suggests that it ought to be possible to stabilize this cation with an appropriate anion. Of course, one of the crucial questions in this matter is the actual magnitude of the binding energy of H_3^+. Since the work described here involves a variational calculation, the only information that can be gleaned from that calculation is that the true binding energy is larger than that, i.e., the calculation has given an <u>upper bound</u> to the true energy. Thus, it is of considerable interest to obtain a <u>lower bound</u>

to the true energy of H_3^+ to "bracket" the true energy. Then much more definitive statements regarding the ability of H_3^+ to combine with suitable anions can be made.

The computation of a lower bound usually is formulated so that matrix elements over the square of the Hamiltonian for the system are needed. In the past, the difficulties in evaluating the integrals that arise in computations of this type have made it impossible to perform such computations except for atoms and the H_2 molecule. No method has been developed for polyatomic molecules. However, we have recently been able to show that, if Gaussian basis orbitals are employed, the integrals can be calculated in closed form or with only a single numerical integration. Fortunately, a very accurate variational wavefunction for H_3^+ using Gaussian basis orbitals has been given by Schwartz.[31] We have succeeded in duplicating his original calculation for the upper bound to H_3^+, and are in the process of developing the necessary computer programs for the use of the Schwartz wavefunction to calculate a lower bound to the ground state energy of H_3^+.

g. Conclusions

(1) The nature of the electronic correlation in the ground state of the H_3^+ molecule has been shown to bear a striking resemblance to its united atom analog (Li^+), by means of an analysis of the occupation numbers arising from a natural orbital analysis.

(2) The main change involved in the transition from the united atom to H_3^+ is that the in-out correlation in the atomic case is transferred to a more formally angular-type

correlation, accompanied by a corresponding change in the first natural orbital from spherical symmetry to the symmetry of the A_1' irreducible representation of the D_{3h} group.

(3) Using the calculated value of -1.2992 hartrees at R = 1.6575 bohrs for the approximate Hartree-Fock energy of H_3^+ as found from the first natural orbital, the Hartree-Fock energy has been estimated to be -1.301 hartrees.

(4) Electron density plots of the square of the first natural orbital have confirmed the earlier speculation that the appropriate way to describe the bonding arrangement in H_3^+ is either by means of bonds pointing toward the center of the molecule from each nucleus, or by means of bent bonds between each pair of nuclei.

(5) If one assumes that the approximately constant value of 0.042 hartrees for the correlation energy of other isoelectronic systems can be taken over to H_3^+, then the total energy of H_3^+ can be estimated to be -1.343 hartrees.

3. GEMINAL THEORY

The work in the area of geminal theory has been focused toward developing an adequate technique for handling many-electron, many-center problems using ab initio principles, but at the same time attempting to retain some degree of intuitive simplicity in the resulting wavefunction. Any theory of chemical binding should account for the highly useful and successful experimental notion that the basic building blocks of normal chemical bonds are <u>pairs</u> of electrons, and not individual electrons acting independently. This is done in geminal theory by assuming that, for an even number of electrons, the total wavefunction can be written as a properly antisymmetrized product of pair functions (geminals);

$$\Phi(1,2,\ldots,2N) = \mathcal{A}G_1(1,2)\cdot G_2(3,4) \ldots\ldots \cdot G_N(2N-1,2N),$$

where each geminal G_i is a normalized, antisymmetric function of the space and spin coordinates of two electrons. Furthermore, each geminal can be as complicated as the user desires, and so can allow for a very careful description of the interaction of two electrons within the same geminal. It is known experimentally that, in many cases, the interaction between two electrons within the <u>same</u> geminal is much stronger than the interaction between electrons in <u>different</u> geminals. This is usually integrated into pair theory via the strong orthogonality constraint, i.e.,

$$\int G^*_\mu(1,i)G_\nu(1,j)d\tau_1 = \delta_{\mu\nu}$$

For computational purposes, each geminal is usually written as a product of a space and a spin part,

$$G_\mu(1,2) = \Lambda_\mu(1,2) \textcircled{H}(1,2),$$

and the space portion is usually expressed in "natural orbital form":

$$\Lambda_\mu(1,2) = \sum_{i=1}^{N_\mu} C_{\mu i}\chi_i(1)\chi_i(2),$$

where $C_{\mu i}$ is the occupation number of the ith natural orbital in the μth geminal, and is to be determined so that the energy is minimized. Of course, the determination of the appropriate natural orbitals χ_i is also done so that the energy is minimized. Within these approximations, the total energy of the space portion of a system consisting of 2N electrons is given by

$$E = \sum_{\mu=1}^{\text{all geminals}} \left\{ 2\sum_{i=1}^{N_\mu} C^2_{\mu i}\langle \mu_i|h|\mu_i\rangle + \sum_{i,j}^{N_\mu} C_{\mu i}C^*_{\mu j}\left[\mu_i\mu_j|\mu_j\mu_i\right] \right\}$$

$$+ \sum_{\mu<\nu}^{\text{all geminals}} \left\{ \sum_{i,j}^{N_\mu,N_\nu} C^2_{\mu i}C^2_{\nu j}\left(4\left[\mu_i\mu_i|\nu_j\nu_j\right] - 2\left[\mu_i\nu_j|\nu_j\mu_i\right]\right) \right\},$$

where $\mu_i = \chi_{\mu i}$, h is a one-electron operator, and

$$\left[\alpha\beta|\gamma\delta\right] = \iint \chi^*_\alpha(1)\chi_\beta(1)\frac{1}{r_{12}}\chi^*_\gamma(2)\chi_\delta(2)\,dV_1\,dV_2.$$

When this expression is minimized with respect to the natural orbital occupation coefficients, subject to the normalization condition, one must solve the following coupled eigenvalue equation to determine $C_{\eta k}$:

$$\sum_i H^{\eta}_{ki} C_{\eta i} = \epsilon_{\eta} C_{\eta k} \quad , \quad \begin{cases} k = 1,2\ldots\ldots, N_{\eta} \\ \eta = 1,2\ldots\ldots, \text{all geminals.} \end{cases}$$

where H^{η}_{ki} is an effective Hamiltonian for the ηth geminal. These equations are coupled, i.e., we need to know all the other C's to solve for $C_{\eta k}$. These equations are usually easily solved via an iterative technique, which begins by making the initial approximation that

$$C_{\eta 1} = 1, \quad C_{\eta j} = 0 \qquad (j > 1),$$

and solving the above equation for ϵ_{η}, and consequently, a new set of $C_{\eta i}$. This procedure is then repeated until the results are self-consistent, i.e., the set of C's does not change from one iteration to the next. This technique is not new, and has proven to be effective in practice.

However, the energy expression must also be minimized with respect to the natural orbitals themselves, subject to the constraint that the natural orbitals remain orthonormal, i.e.,

$$\int \chi^*_{\mu i}(1)\, \chi_{\nu j}(1)\, dV_1 = \delta_{\mu\nu} \cdot \delta_{ij}.$$

When this minimization is carried out, we obtain the following set of coupled integro-differential equations for the determination of the natural orbital $\chi_{\mu i}$:

$$\left\{ C_{\mu i}^2 h + \sum_{j=1}^{N_\mu} C_{\mu i} C_{\mu j}^* K_{\mu j} + \sum_{\substack{\text{all geminals} \\ \nu(\neq\mu)}} \sum_{j=1}^{N_\nu} C_{\mu i}^2 C_{\nu j}^2 \left[2J_{\nu j} - K_{\nu j} \right] \right\} \chi_{\mu i}$$

$$= \sum_{\substack{\text{all geminals} \\ \nu=1}} \sum_{j=1}^{N_\nu} \lambda_{\mu i, \nu j} \chi_{\nu j} ,$$

where

$$J_{\nu j} = \int \chi_{\nu j}^*(2) \chi_{\nu j}(2) \frac{1}{r_{12}} dV_2 ,$$

$$K_{\nu j}(1) \chi(1) = \int \chi_{\nu j}(1) \chi_{\nu j}^*(2) \frac{1}{r_{12}} \chi(2) ,$$

and the $\lambda_{\mu i, \nu j}$ are Lagrangian multipliers which arise from the orthogonality constraints. Due primarily to the fact that "off-diagonal" Lagrangian multipliers ($\lambda_{\mu i, \nu j}$, with $\mu i \neq \nu j$) appear in the equations, there has not to date been a successful algorithm developed for the solution of these equations. However, it is shown below that it is possible to develop a workable algorithm for the solution of these equations by first transforming the equations to a simpler, but entirely equivalent form.

We first let

$$M_{op}(\mu i) = C_{\mu i}^2 h + \sum_{j=1}^{N_\mu} C_{\mu i} C_{\mu j}^* K_{\mu j} + \sum_{\substack{\text{all geminals} \\ \nu(\neq\mu)}} C_{\mu i}^2 C_{\nu j}^2 \left[2J_{\nu j} - K_{\nu j} \right] ,$$

and rewrite the equations determining the natural orbitals in matrix form,

$$M_{op}\,\underline{\chi} = \underline{\lambda}\,\underline{\chi}\,,$$

where $\underline{\chi}$ is a column vector, given by

$$\underline{\chi} = \begin{pmatrix} \chi_{11} \\ \chi_{12} \\ \vdots \\ \chi_{1N_1} \\ \chi_{21} \\ \vdots \\ \chi_{QN_Q} \end{pmatrix},$$

where Q is the number of geminals, and

$$\underline{\lambda} = \begin{pmatrix} \lambda_{11,11} & \lambda_{11,12} & \cdots & \lambda_{11,1N_1} & \lambda_{11,21} & \cdots & \lambda_{11,QN_Q} \\ \lambda_{12,11} & \lambda_{12,12} & & & & & \vdots \\ \vdots & & & & & & \vdots \\ \lambda_{QN_Q,11} & \cdots & & & & & \lambda_{QN_Q,QN_Q} \end{pmatrix}.$$

We now note that $\underline{\lambda}$ is a real, symmetric matrix. This is apparent from the fact that $\lambda_{\mu i,\nu j}$ and $\lambda_{\nu j,\mu i}$ both arise from the <u>same</u> orthonormality constraint,

$$\int \chi^*_{\mu i}\,\chi_{\nu j}\,dV = \int \chi^*_{\nu j}\,\chi_{\mu i}\,dV = \delta_{\mu\nu}\cdot\delta_{ij}\,,$$

and consequently $\lambda_{\mu i,\nu j}$ must be identical to $\lambda_{\nu j,\mu i}$. With this information,

we note that any real, symmetric matrix can be brought to diagonal form via a unitary transformation. Denoting this transformation by U, we can rewrite the equations to be solved as:

$$\underline{U}\, M_{op}\, \underline{\chi} = \left(\underline{U}\, \underline{\lambda}\, \underline{U}^{+}\right) \underline{U}\, \underline{\chi}\,,$$

or

$$M_{op}\underline{\chi}' = \underline{\lambda}'\underline{\chi}', \text{ or } M_{op}\chi'_{\mu i} = \epsilon_{\mu i}\chi'_{\mu i}$$

where $\underline{\lambda}' = \underline{U}\,\underline{\lambda}\underline{U}^{+}$ = diagonal matrix, $\lambda_{\mu i,\mu i} = \epsilon_{\mu i}$, and $\underline{\chi}' = \underline{U}\underline{\chi}$. The diagonalization of the original $\underline{\lambda}$ matrix provides a considerable simplification, because it removes the off-diagonal Lagrang'an multipliers from the problem, and decouples the equations determining the natural orbitals. The solution must still be done in an iterative manner, since $M_{op}(\mu i)$ depends upon a knowledge of all of the other natural orbitals. However, the iterative nature of the solution is entirely similar to that which arose in the determination of the natural orbital occupation coefficients, $C_{\mu i}$, and it is anticipated that the transformation introduced here will allow the determination of the natural orbitals to be carried out just as easily as the determination of the occupation coefficients. The implementation of the computer programs representing this approach is in progress, and a quantitative estimate of the time that will be saved by this analysis is being sought.

Although considerable progress has been made toward development of a suitable algorithm for solving the equations which determine the geminals, geminal theory itself cannot be considered to be a general theory unless

the restriction to systems with an even number of electrons can be removed. As shown below, it is indeed possible to generalize geminal theory to include an odd electron.

Consider a system of 2N+1 electrons, in which 2N of the electrons are spin paired. The trial function is written as a properly antisymmetrized product of N geminals and one orbital:

$$\psi(1,2,\ldots,2N,2N+1) = A\left\{G_1(1,2)G_2(3,4)\ldots G_N(2N-1,2N)\Phi(2N+1)\right\}$$

In a manner similar to that in which the individual geminals are treated, the space portion of the added orbital can be expanded in terms of natural orbitals, i.e.,

$$\Phi(N+1) = \sum_{i=1}^{N_{N+1}} C_{(N+1)i}\chi_{(N+1)i} ,$$

with

$$\int \chi^*_{(N+1)i}\chi_{(N+1)j}dV = \delta_{ij} .$$

The strong orthoganality constraint is generalized to include

$$\int \Lambda^*_\mu(1,2)\Phi(1)dV_1 = 0, \quad \mu = 1,2,\ldots\ldots N.$$

With this form of the wavefunction, the total energy of the system of 2N+1 electrons can be shown to be

$$
{}^2E = \sum_{\mu=1}^{N}\left\{2\sum_{i=1}^{N_\mu} C_{\mu i}^2 \; (\mu_i|h|\mu_i) + \sum_{i,j}^{N_\mu} C_{\mu i} C_{\mu j}\left[\mu_i\mu_j|\mu_j\mu_i\right]\right\}
$$

$$
+ \sum_{i,j} C_{(N+1)i} C_{(N+1)j} \left((N+1)i\,|\,h\,|\,(N+1)j\right)
$$

$$
+ \sum_{\mu<\nu}^{N}\left\{\sum_{i,j} C_{\mu i}^2 C_{\nu j}^2\left(4\left[\mu_i\mu_i|\nu_j\nu_j\right] - 2\left[\mu_i\nu_j|\nu_j\mu_i\right]\right)\right\}
$$

$$
+ \sum_{\mu=1}^{N}\left\{\sum_{i}\sum_{j,k} C_{\mu i}^2 C_{(N+1)j} C_{(N+1)k}\left(2\left[\mu_i\mu_i\,|\,(N+1)_j(N+1)_k\right] - \left[\mu_i(N+1)_k\,|\,(N+1)_j\mu_i\right]\right)\right\}.
$$

By comparison with the previous energy expression for a system in a singlet state with an even number of electrons, it is seen that the additional terms result from the intergeminal interactions caused by the presence of the additional orbital.

As in the singlet case, the energy expression must also be minimized with respect to both the best natural orbital expansion coefficients and the natural orbitals themselves. When this procedure is carried out for the doublet case equations analogous to those of the singlet case, but slightly more complicated due to the presence of the additional intergeminal terms, are obtained. However, the techniques that have been developed for the singlet case are directly applicable.

Thus the analysis which is necessary to generalize geminal theory for use on systems of possible interest as propellants is completed, as well as a new algorithm for the computation of the geminals which describe these systems. Work is underway to implement this analysis with the appropriate computer programs.

4. REFERENCES

1. H. Shull, J.A.C.S., 82, 1287 (1960).
2. H. Shull, J. Phys. Chem., 66, 2320 (1962).
3. S. Hagstrom and H. Shull, Rev. Mod. Phys., 35, 624 (1963).
4. H. Shull and F. Prosser, J. Chem. Phys., 40, 233 (1964).
5. H. Shull, J.A.C.S., 86, 1469 (1964).
6. B. Anex and H. Shull, "Molecular Orbitals in Chemistry, Physics, and Biology", edited by P. O. Löwdin and B. Pullman, (Academic Press, 1964), p. 227.
7. D. R. Hartree, Proc. Camb. Phil. Soc., 24, 89 (1928); V. Fock, Zeit. f. Physik, 61, 126 (1930).
8. See, for example: R. K. Nesbet, "Advances in Chemical Physics", edited by I. Prigogine (Interscience Publishers, Inc., 1964), Vol. 9, p. 321, and references therein.
9. P. O. Löwdin, "Advances in Chemical Physics", edited by I. Prigogine, (Interscience Publishers, Inc., 1959), Vol. 2, p. 209.
10. H. Shull, J. Chem. Phys., 30, 1405 (1959).
11. R. E. Christoffersen, J. Chem. Phys., 41, 960 (1964).
12. G. P. Barnett, J. Linderberg and H. Shull, J. Chem. Phys., 43S, 80 (1965).
13. P. O. Löwdin and H. Shull, Phys. Rev., 101, 1730 (1956).
14. A. Macias, to be published.
15. A. Weiss, Phys. Rev., 122, 1826 (1961).
16. W. A. Lester, Jr. and M. Krauss, J. Chem. Phys., 44, 207 (1966).
17. H. Preuss, Zeit. f. Natur., 20, 21 (1965).
18. B. D. Joshi, J. Chem. Phys., 44, 3627 (1966).
19. H. Shull and P. O. Löwdin, J. Chem. Phys., 23, 1565 (1955).
20. G. V. Nazaroff and J. O. Hirschfelder, J. Chem. Phys., 39, 715 (1963).

21. S. Peyerimhoff, J. Chem. Phys., 43, 998 (1965).

22. W. Kolos and C. C. J. Roothaan, Rev. Mod. Phys., 32, 219 (1960).

23. P. O. Löwdin, "Advances in Chemical Physics", I. Prigogine, ed., (Interscience Publishers, 1959), vol. 2, p. 207.

24. A. W. Weiss, Phys. Rev., 122, 1826 (1961).

25. H. Conroy, J. Chem. Phys., 41, 1341 (1964).

26. H. Michels, J. Chem. Phys., 44, 3834 (1966).

27. L. Wolniewicz, J. Chem. Phys., 43, 1087 (1965).

28. A. D. McLean, A. Weiss, and M. Yoshimine, Rev. Mod. Phys., 32, 211 (1960).

29. This effect has also been noticed (without comments concerning the bonding description) by A. G. Pearson, R. D. Poshusta and J. C. Browne, J. Chem. Phys., 44, 1815 (1966).

30. G. S. Handler and J. R. Arnold, J. Chem. Phys., 27, 144 (1957).

31. M. Schwartz, Ph.D. Thesis, Vanderbilt University, 1966.

II. MICROWAVE SPECTROSCOPY OF TRANSIENT ENERGETIC SPECIES

1. INTRODUCTION

Our microwave spectroscopic studies have as their goal the elucidation of the structure, reactivity, and energetics of gaseous free radicals and excited-state molecules. While a considerable amount of work has been carried out by optical absorption and emission studies, very little microwave spectroscopy has been performed on these unstable species. The advantages of this technique may be summarized as follows.

(a) The microwave technique is the most suitable for structural determinations. This information is needed for the calculation of the thermodynamic properties of the unstable species, and for an understanding of the mechanism of their formation and reactions.

(b) The microwave technique is a suitable means for detection of low concentrations of gas-phase species.

(c) Microwave spectroscopy lends itself well to double-irradiation methods; for example, it is possible to irradiate a sample with ultraviolet radiation while simultaneously observing its microwave spectrum.

In the following sections we have summarized the microwave studies that have been undertaken. Much of the work to date has involved the design, construction and testing of a spectrometer suitable for the proposed studies, so these aspects have been discussed in some detail. Some preliminary studies of biacetyl photosensitization have also been discussed, and our initial attempts to produce and detect free radicals have been outlined.

2. SPECTROMETER CONSTRUCTION

a. The Complete Spectrometer

In Figure II-1 a block diagram of the spectrometer is presented. In the following we will give more detail about some of the components. The klystrons, waveguide components and detector are standard items. At present, our frequency range is 8 GHz to 30 GHz. The klystron power supply is a PRD universal type 812 and is capable of supplying any klystron that we might need. Lock-in (or phase sensitive) detection is accomplished by means of a PAR model JB-5 lock-in amplifier which operates between 10 cps and 100 kc/s. Some pre-amplification is performed by means of a narrowband amplifier tuned at the reference frequency. Spectrum observation is performed by use of either the Tektronix type 502A dual-beam oscilloscope or the Bausch and Lomb VOM-6 recorder. Signal modulation of paramagnetic species is produced by the Zeeman modulator built and designed in our labs. This unit produces a magnetic field of up to 5 to 10 gauss in the solenoid at a frequency of 1 kc/s. Rise and fall times of the 1 kc/s square-wave are about 10%, and the bottom of the square wave is zero-based. Figure II-1 presents a circuit diagram of this unit. The sample-cell, quartz rod transmission system and modulation coil are discussed in more detail in the following section.

b. Sample Cell Design

Figure II-2 presents a sketch of the cell and quartz rod transmission system. The principles of this type of dielectric rod

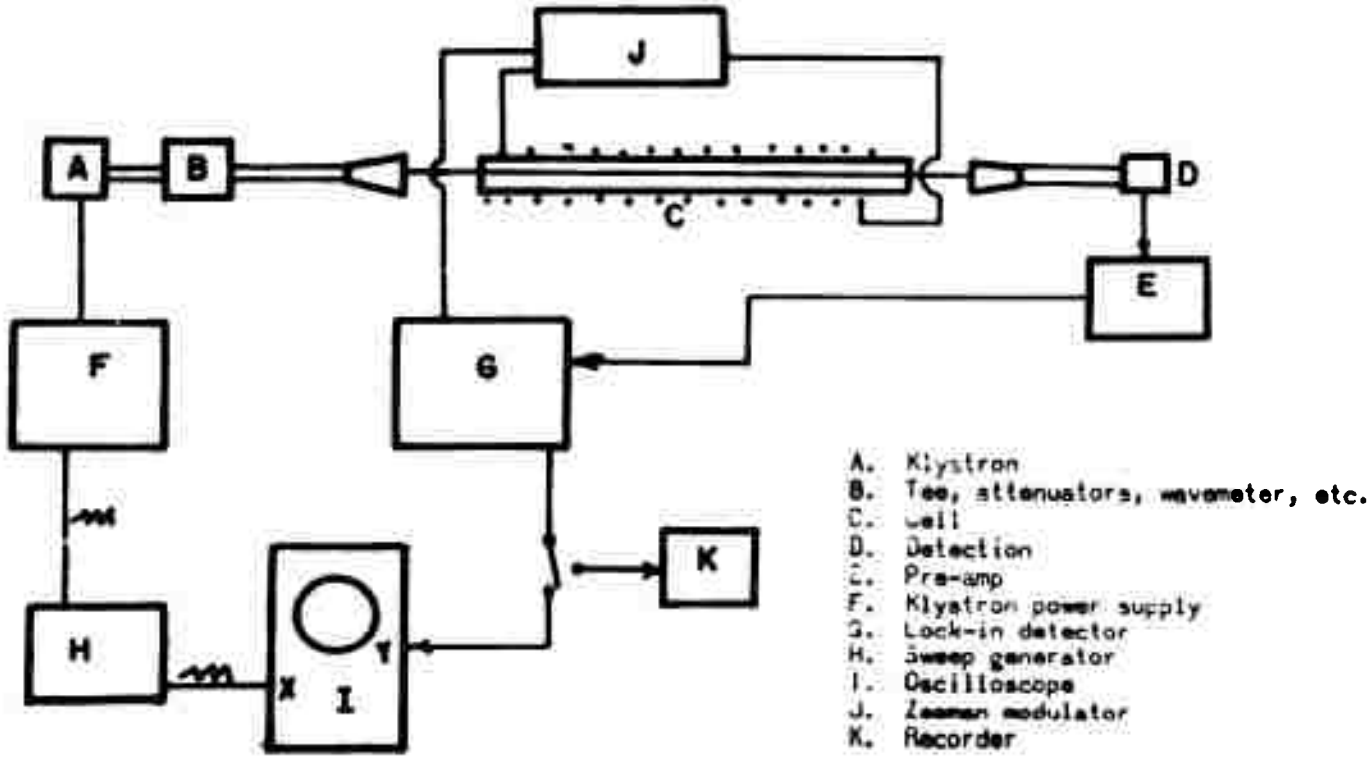

Figure II-1. Spectrometer - block diagram.

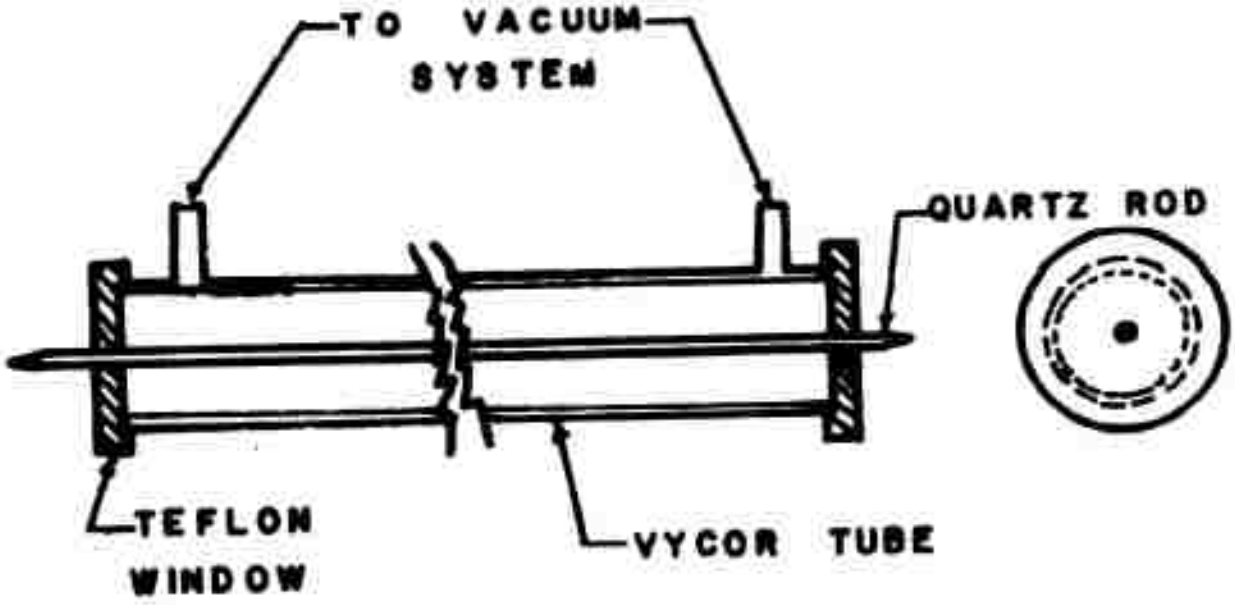

Figure II-2. Sample cell.

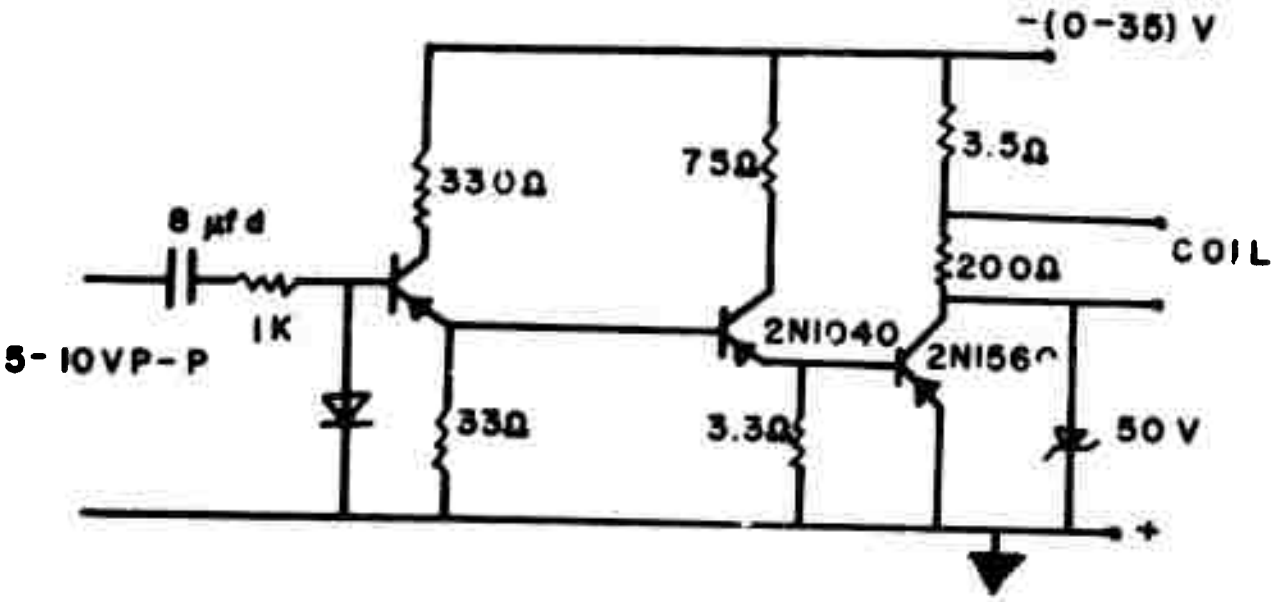

Figure II-3. Prototype Zeeman Modulator.

transmission system have been discussed by Brackett et al.[1] By choosing the rod diameter properly, the system can be made to transmit useable microwave power over any frequency range of interest. The hybrid TEM mode is easily excited from a waveguide system by means of standard microwave horns. Figure II-4 presents a graph which shows the useable power (that which is outside of the quartz rod but within the quartz cell) as a function of frequency for three different rod diameters.

At the present time the teflon windows are sealed to the quartz tube by means of Apiezon W wax, while the vacuum seal between the rod and the window is produced by paraffin. The use of O-rings is being contemplated in place of Apiezon W, but at present this modification has not been undertaken.

The Vycor tube is the major component of the sample cell; its nominal dimensions are 3 feet x $1^{13}/_{16}$ inch. Since Vycor transmits into the near UV, external irradiation of samples is possible. The cell is attached to a high-speed pumping system so that continuous flow techniques are possible.

Zeeman modulation is produced by the solenoid wrapped around the sample cell. The coil is made from 16 gauge copper wire and has about 4 turns/inch over a length of 30 inches.

c. Spectrometer Tests

Before mentioning the results using Zeeman modulation, a few comments about Stark (electric field modulation) seem in order. Using a smaller diameter sample cell, a 5 Kc/s square wave voltage was applied to two aluminum plates (3" X 30" X $^1/_{16}$") placed parallel to the axis of the cell and to each other. With our square wave generator it was possible to obtain an electric field of 500 volt/cm. Some OCS absorption lines in the

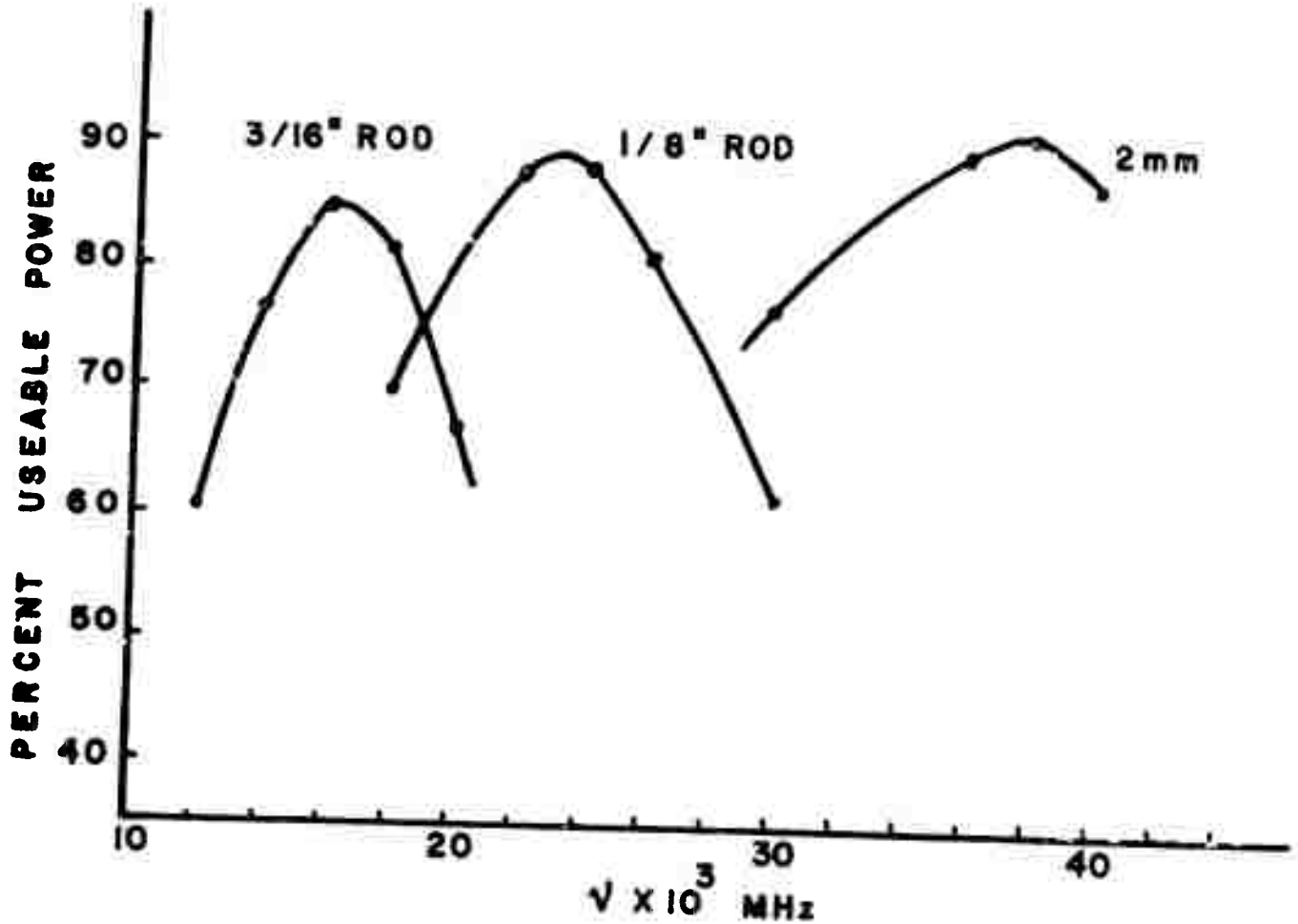

Figure II-4. Dielectric rod transmission.

vicinity of 24325 Mc/s were observed with this arrangement, but the sensitivity was very poor. It was only 1×10^{-6} cm^{-1} (minimum detectable absorption coefficient), compared to about 5×10^{-9} for standard Stark spectrometers. This very poor sensitivity was evidently caused by poor modulation resulting from charges built up on the Vycor surfaces. It seems evident that the arrangement is not satisfactory so Stark modulation methods will be of little use. Because we are interested in paramagnetic species, no further work along this line is contemplated.

Our first satisfactory Zeeman modulation spectrum has been obtained by using NO_2 as the test sample. Six of the eight hyperfine components[2] of the $J = 23_{2,22} \longrightarrow J = 24_{1,23}$ transition at 26,600 MHz have been observed with S/N of about 50/1. This places our present spectrometer sensitivity between 1×10^{-7} and 1×10^{-8}. These res s are very encouraging, since we now have under construction a quality Zeeman modulator which will operate in the 10-20 Kc/s range. Assuming that crystal noise predominates, the new unit should produce a sensitivity increase of a factor of $\sqrt{10}$ or $\sqrt{20}$, i.e., about 3 or 4. In fact, greater enhancements are expected, since the rise and fall times will be only about 3% for the new unit, whereas the unit of Figure II-3 has very poor rise and fall characteristics. Table II-I gives a summary of the specifications for the Zeeman modulation unit now under construction; the first tests are expected to be made in December, 1967. It seems not unreasonable to expect sensitivities of greater than 1×10^{-8} cm^{-1} when the new modulator is put into operation.

Experiments for the detection of OH radical are now underway, since these will provide a more stringent test of our apparatus. The Λ-doublet transitions which occur at about 23822 MHz[3] will be utilized for detection

TABLE II-1. New Zeeman Modulator Specifications

Power required:	75 watts max
Maximum coil inductance:	400 μH
Frequency:	Variable to 20 KHz
Rise and fall time:	3 μ sec each at 10 KHz
Drive current:	4 amps max
Waveform flatness:	Better than ± 3%
Zero-basing of waveform:	To within 1 ma

purposes. OH radicals will be produced by use of a 2500 MHz microwave discharge by one of the following systems:

$$H_2 + O_2 \xrightarrow{\text{discharge}} OH + \ldots \qquad (1)^3$$

$$H + NO_2 \longrightarrow OH + NO \qquad (2)^4$$

$$H_2O + H_2O_2 \xrightarrow{\text{discharge}} OH + \ldots \qquad (3)^5$$

The radical production will be made continuous by using the rapid flow technique previously mentioned.

We plan to detect SO radicals with our Zeeman spectrometer also; previous workers[4] have observed several transitions using Stark modulation, but no magnetic studies were performed.

3. INITIAL STUDIES

a. Free Radicals

The first attempt at detecting a new free radical will be performed on the CF_3 species. $CF_2(^1A)$ has been detected by Powell and Lide[6] as a product of electrodeless discharges in a variety of fluorinated molecules including $(CF_3)_2CO$. We will search for the symmetric rotor spectrum of CF_3 produced by flowing perfluoroacetone through a microwave discharge. It seems highly unlikely that this free radical will have zero dipole moment, and it is expected to exhibit its $J = 0 \rightarrow J = 1$ transition in the neighborhood of 20 GHz. It should be noted that absorption lines of non-paramagnetic species will not be observed with the Zeeman system, so that the parent molecule spectrum will cause no difficulty.

A search will also be carried out for the spectrum of the PO ($^2\pi$) radical. This species was recently observed[7] in emission by passing phosphorus vapor and oxygen through a 2450 MHz microwave discharge. Although the $J = 0 \longrightarrow J = 1$ transition is beyond our frequency range (at about 45 GHz), there is some hope of observing magnetic dipole transitions at lower frequencies.

For radical studies in which it is desired to mix the products of the discharge with another species, we use the arrangement shown in Figure II-5. This arrangement is useful, for example, in producing OH by mixing NO_2 with H atoms produced by dissociation of H_2 in the discharge.

b. Electronically Excited Species

Preliminary experiments that we have performed show that the production of triplet biacetyl may be efficient enough to permit the observation of its microwave spectrum. The method is as follows. Triplet naphthalene is formed by relatively strong irradiation at 2537 Å of ground state naphthalene, followed by intersystem crossing from the excited singlet system. Collisions of the second kind between singlet biacetyl and triplet naphthalene produce triplet biacetyl.

The above photosensitization reaction has been observed semi-quantitatively in the following manner. A mixture of biacetyl and naphthalene has been irradiated at 2537 Å. The emission of the sample has been observed with a Bausch and Lomb monochromator and has been found to contain only the green biacetyl phosphorescence; no biacetyl fluorescence is observed. This clearly indicates that energy transfer occurs as described above, and not

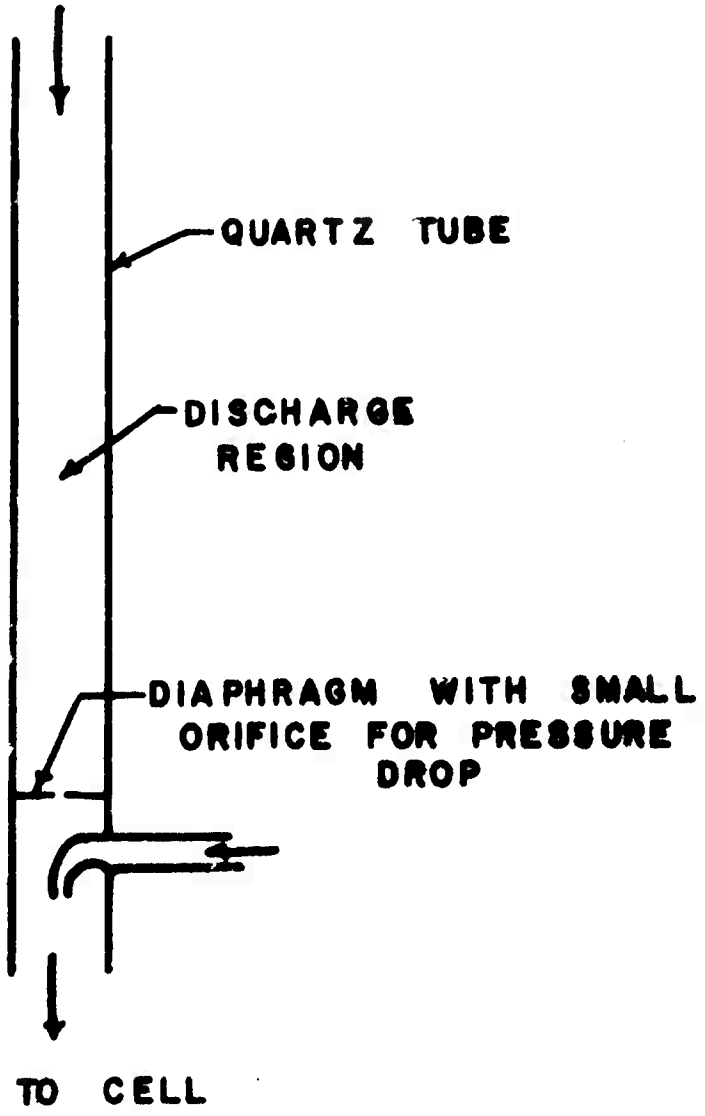

Figure II-5. Discharge and mixing tube.

by transfer of excited singlet energy between the molecules. Experiments to determine the quantum efficiency of this process are underway and will be ready for publication in a short time.

The microwave experiments will be performed by passing a mixture of biacetyl and naphthalene through the cell while irradiating with mercury resonance lamps. Crude calculations indicate that about 10^{20} photons/sec of 2537 Å radiation will be sufficient to produce detectable amounts of triplet biacetyl. Lamps are available which supply this much radiation, but they will have to be specially fabricated to achieve such intensities over our geometric configuration.

4. REFERENCES

1. E. B. Brackett, P. H. Kasai and R. J. Myers, Rev. Sci. Instrum., 28, 699 (1957).

2. G. R. Bird, J. Chem. Phys., 25, 1040 (1956).

3. G. C. Dousmanis, T. M. Sanders and C. H. Townes, Phys. Rev., 100, 1735 (1955).

4. F. X. Powell and D. R. Lide, J. Chem. Phys., 41, 1413 (1964).

5. D. R. Johnson and C. C. Lin, J. Mol. Spectrosc., 23, 201 (1967).

6. F. X. Powell and D. R. Lide, J. Chem. Phys., 45, 1067 (1966).

7. N. L. Singh, Can. J. Phys., 37, 136 (1959).

III. RADIATION-INDUCED CHARGE STORAGE IN ORGANIC POLYMERS

1. INTRODUCTION

The primary interaction of gamma rays of energies between 0.3 and 3 Mev with matter is the Compton process. Electrons scattered by this mechanism leave positive holes and move through the medium causing additional ionization and excitation until they either recombine or are trapped. Likewise positive holes are free to move in some materials until they are neutralized or trapped. Charge carriers which are stabilized in a solid medium can be described as trapped in a potential well. The charges may be detrapped by thermal or photo excitation. The detrapped, mobile charges can be used to probe the cross-section for retrapping which relates to the nature of the trapping site, the spatial distribution of trapping sites, the mobility mechanism and the limiting density of trapped charges.

It is of importance to study both trapped and mobile charges in order to properly assess the feasibility of storing large amounts of charge for possible rocket propellants. In the present program this is being achieved by thermally generated currents in irradiated organic solids. The development of electron paramagnetic resonance studies of trapped charges, reactivity studies of mobile ions in the liquid phase and mobility measurements of electrons and holes in irradiated solids is also being implemented.

Thermal heating can be used to detrap charges in irradiated solids. If a temperature gradient is applied across the sample the charges will preferentially drift in one direction and create an observable current. Such currents are called thermoelectric currents. Hardtke[1] reports the

observation of thermoelectric currents of a few picoamperes when samples of cabal glass are irradiated by cobalt-60 and then heated in temperature gradients approximating 30°C/mm. He also reports observing the same phenomenon in certain other dielectrics including polystyrene and nylon. Gross[2] measured similar currents under similar temperature gradients in borosilicate glass.

Experimentally, one can consider two classes of organic systems to be studied. In the first class are rather simple organics such as 3-methylpentane, triethylamine, etc., which are liquids or gases at room temperature, and which must be frozen and irradiated at temperatures down to 4°K in order to trap ions. In this class exploratory work is beginning on triethylamine. The second class are organic solids which can trap charge at room temperature and above; these are usually polymeric systems.

Charge storage in polymethylmethacrylate (PMMA) has been investigated by Barnes.[3] He found that a voltage was generated across an irradiated Lucite sample when heated. This suggested that charges were trapped in the irradiated Lucite and that this material would be a fruitful system for further study. The results obtained here by Barnes in a subsequent, independent investigation bear this out. By using pure PMMA as well as PMMA doped with hole and electron traps we have discovered that added electron traps but not hole traps lead to charge stabilization. We have further found that polymers containing built-in electron traps, such as polyvinyl chloride (PVC), stabilize even larger amounts of charge. It is of considerable significance that the stored charge can be obtained as a thermoelectric current by application of extremely small temperature gradients of ~5°/cm. The requirements for charge stabilization in irradiated organic polymers at relatively high temperatures are beginning to emerge.

2. EXPERIMENTAL

a. Sample Preparation

Samples of the organic polymers under investigation were machined into disks, normally 2.5 cm in diameter and 1 cm thick, from cylindrical stock. This geometrical shape facilitated the attachment of electrodes and the maintenance of a clean insulating surface between the electrodes.

The flat surfaces of the disks were coated with a low resistance conductive cement for plastics, Eccobond Solder 56C, to serve as electrodes. Eccobond Solder (Emmerson and Cummings, Inc.) is a silver-colored paste to which a No. 11 catalyst is added for hardening. Cure of the coated surfaces was accomplished in 4 hours at 65°C.

The Eccobond solder also provided a method of attaching 3/4 inch metal tabs to the flat surfaces of the disks. These tabs were opposite each other and allowed to protrude 1/2 inch from the edge of each electrode. Each tab provided a means of handling the sample by one electrode at a time without shortcircuiting the two electrodes.

The primary organic polymer studied was polymethylmethacrylate (PMMA).

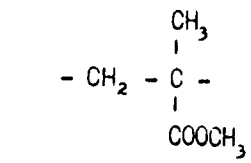

monomer M.W. = 100.11

This polymer is available commercially under the trade names of Lucite, Plexiglas, Diakon, Perspex and Crystalite. Usually the commercial polymerization involves the use of benzoyl peroxide as a chemical initiator and some benzoyl peroxide is present in trace quantities in the final product.

In addition to commercial PMMA, studies were made of material polymerized from pure monomer. Various chemical compounds including carbon tetrachloride, benzene, chlorobenzene, benzoyl peroxide and 2-methylpentene-1 were added to the monomer in small concentrations before polymerization. Carbon tetrachloride is a good electron scavenger and 2-methylpentene-1 is a positive hole trap.[4]

Other materials studied include polyvinyl chloride (polychloroethylene), polyethylene, polytetrafluoroethylene (Teflon), and triethyleneglycol dimethacrylate (Tedma). All of these materials were obtained from commercial stock except Tedma which was thermally polymerized from the pure monomer. It was necessary to heat the polyvinyl chloride samples to 90°C for 30 minutes in short circuit to remove residual charge carriers trapped in the material by the polymerization process. This preheat treatment was not necessary for any of the other materials studied.

b. Current Measurement

The disk-shaped samples were held during heating and current measurement in a three-sided Teflon sample holder (Figure III-1) between two brass screws, one of which was moveable. Small copper disks were soldered to the heads of each brass screw to provide a smooth flat surface for physical and electrical contact with the sample electrodes. Banana plugs were used to connect the brass screws with the remainder of the current measuring circuit. An additional electrical connection was made to the metal tab on each sample electrode by a copper wire soldered to the brass screw and spots soldered to the tab.

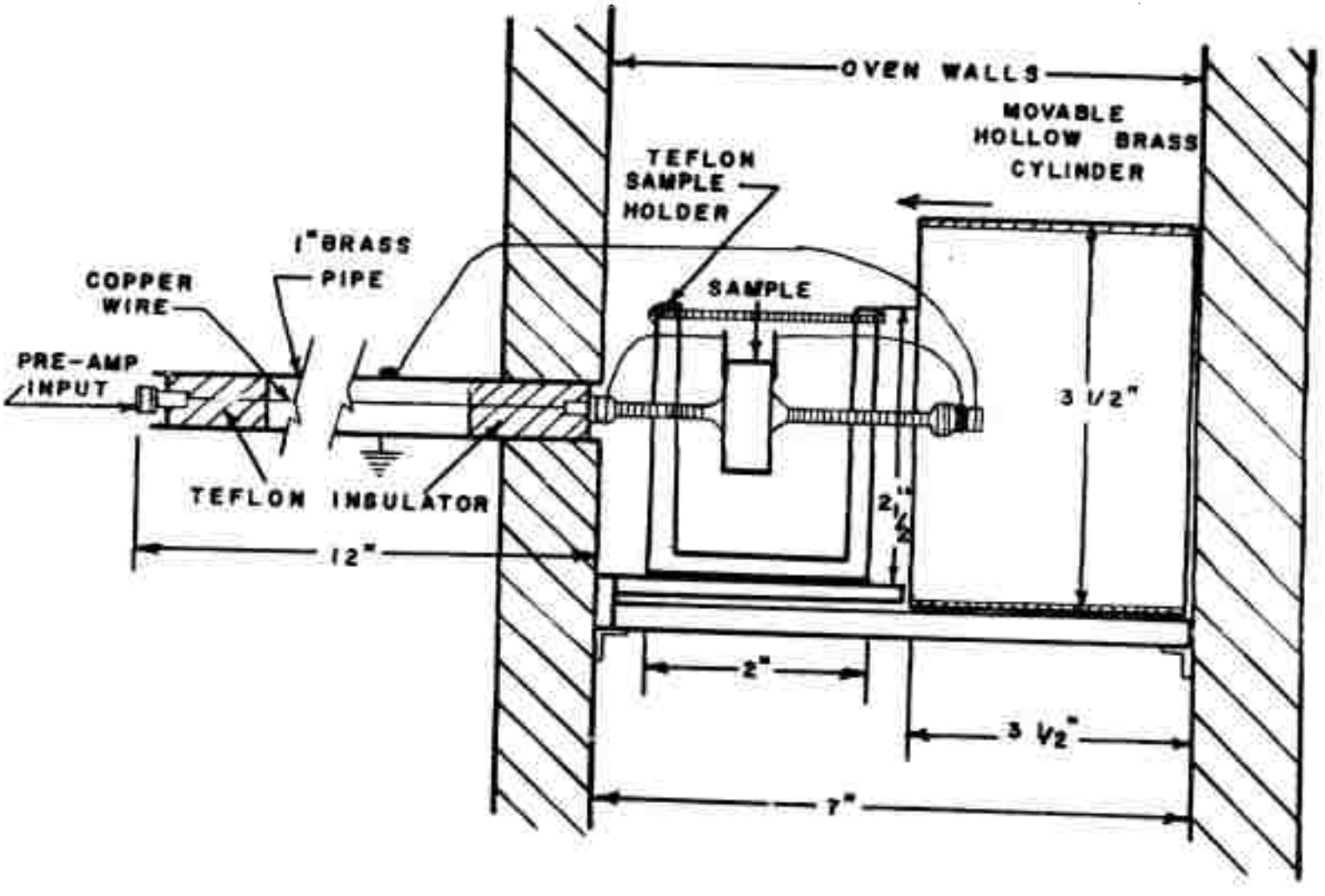

CURRENT MEASURING CONFIGURATION

Figure III-1. Teflon sample holder.

During measurements, the sample holder rested on a brass platform with one electrode connected to the preamp input plug. The other electrode was returned by a heavy multistranded wire to the electrometer ground. After placement of the sample holder in the oven a grounded brass cylinder was moved over it to serve as a guard ring and to control the flow of heated air circulated by the oven fan. The brass cylinder can be considered to be a Faraday cage and therefore supplies capacitive and inductive shielding to the sample and sample holder.

The oven fan was centered in the top of the oven directly over one of the two toroidal shaped 800 watt oven heaters. The other oven heater was located in the bottom of the oven. The hot air circulated by the fan moved downward heating the grounded brass screw which protruded slightly from the end of the brass cylinder. The other brass screw was connected to the input plug which acted as a heat sink thus cooling that side of the sample holder and sample. This heating and cooling resulted in the temperature gradient utilized in this investigation.

The input plug consisted of a 12 inch long, 1 inch diameter brass pipe, three teflon insulators and a heavy copper wire center conductor. The purpose of this plug was to prevent heating of the electrometer preamplifier. The outer brass cylinder was connected to the electrometer ground and helped reduce noise in the system.

c. Temperature Measurement

Figure III-2 is a block diagram of the thermoelectric current measuring circuit. The rate of heating in the oven was controlled by a Varian Aerograph Model 326 linear temperature programmer. Linear heating rates from

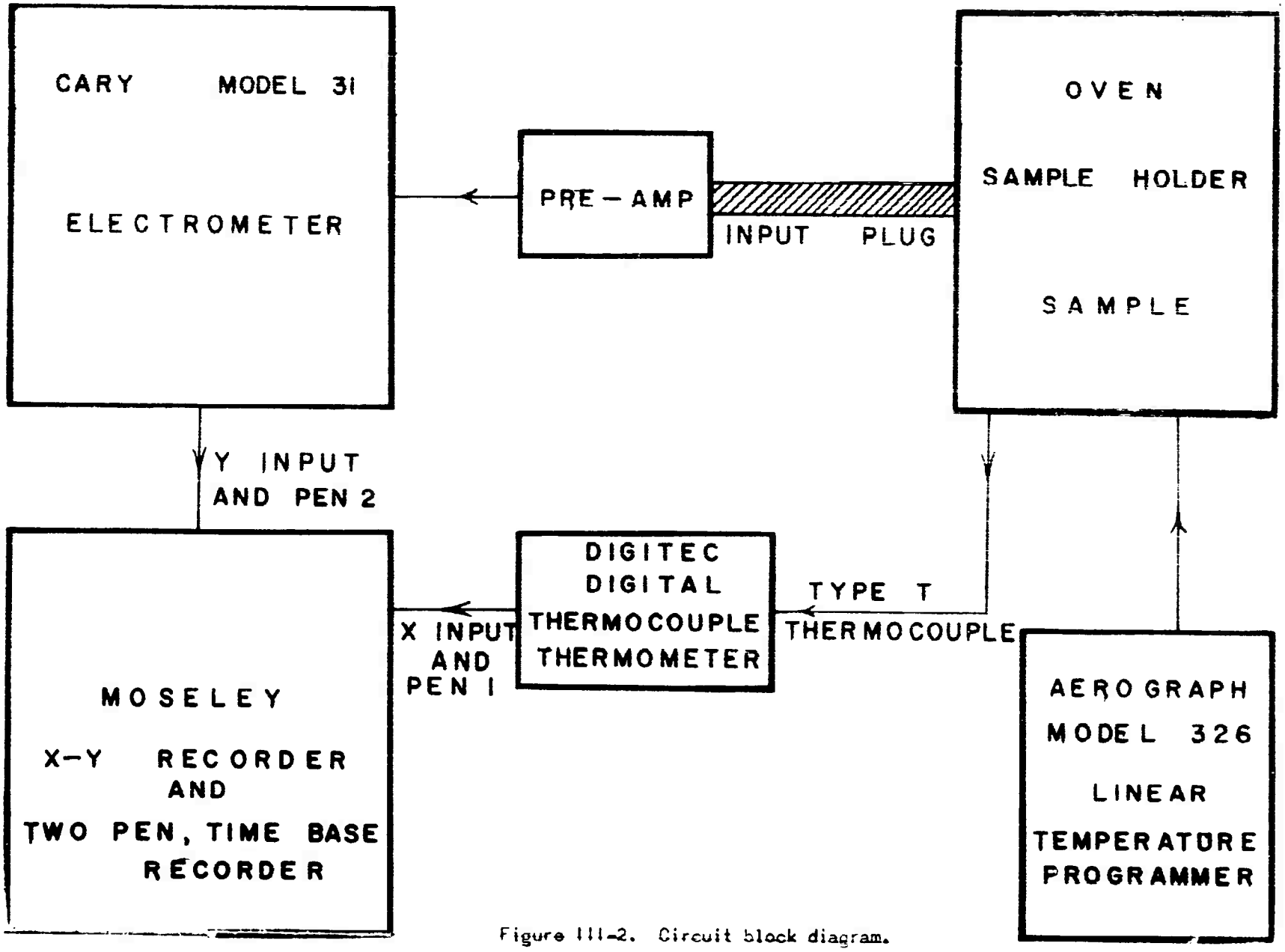

Figure III-2. Circuit block diagram.

$2^{o}C/min$ to $40^{o}C/min$ can be selected. For most measurements a rate of $6^{o}C/min$ was employed.

The temperature of the oven was sensed by a copper-constantan thermocouple soldered to the small copper disk which made contact with the hotter sample electrode. This was on the grounded stationary electrode of the sample holder. The leads of this thermocouple were spliced with a plug-jack connection inside the oven so the sample holder was removable. The potential difference generated at the thermocouple junction was measured by a Digitec Model 564 digital read-out thermometer. This provided an accurate continuous measurement of the temperature of the grounded sample electrode. The signal from this thermocouple was also used as the input for the X-axis of the X-Y recorder.

The thermoelectric currents which were obtained by heating the samples of organic polymers were measured with a Cary Model 31 vibrating-reed electrometer. An input resistance of 10^{10} ohms was used for all measurements and a signal proportional to the magnitude of the current was generated. This signal was plotted against temperature on a Moseley Model 2 FRAM X-Y recorder. Simultaneously, plots of current versus time and temperature versus time were made on a Moseley Model 7100A two pen, time base recorder. Integration of the current versus time plot yielded values proportional to the normalized total charge released in the sample.

At high temperatures thermal stresses in the samples produce noise which mask the thermoelectric current. This noise occurs at a high frequency and can be filtered out to leave only the slowly changing thermoelectric current. Figure III-3 shows the filtering circuit used on the recorder input signal. It is a simple RC circuit with a variable time constant, 0-10 seconds.

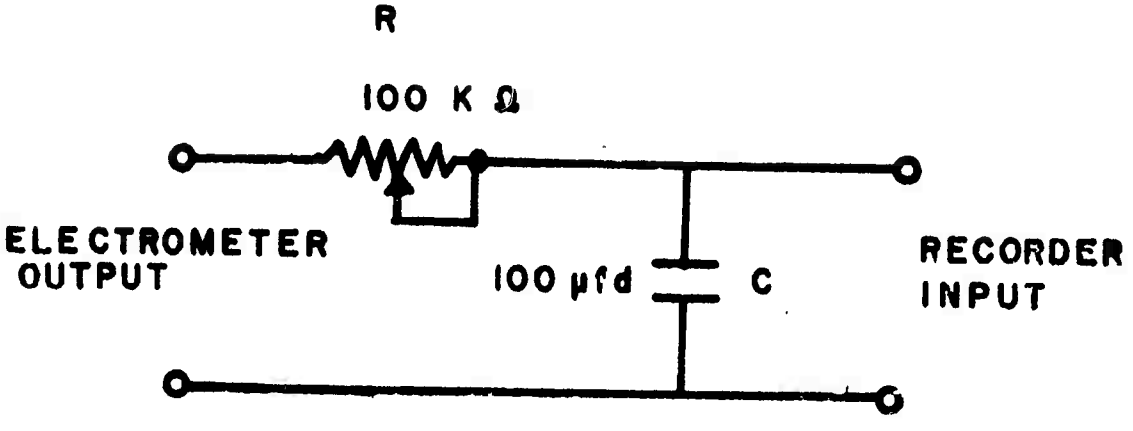

Figure III-3. Noise filtering circuit.

For a very fast rising peak a slight distortion will result but, assuming the peak is symmetrical, the area under the curve will be unchanged.

d. Temperature Gradients

The temperature gradient across the sample was measured by using Eccobond solder to attach copper-constantan thermocouples directly to the conducting electrodes of an unirradiated sample. The potential generated by each thermocouple was selected by a switching arrangement and measured by a Leeds and Northrup potentiometer. Standard conversion tables for thermocouples were used to correlate the observed potentials with the corresponding temperatures. Values for the two electrodes were subtracted, divided by the sample thickness, and then plotted against time to obtain temperature gradient curves. Figure III-4 shows the results of such a temperature gradient measurement on a sample 1 cm thick. Figure III-5 shows a similar temperature gradient measurement on a thin sample 0.1 cm thick.

In order to test the postulate that the temperature gradient caused the flow of measured thermoelectric current, measurements were made on samples heated in the absence of a temperature gradient. Some experimentation showed that by moving the sample, sample holder and brass guard cylinder to the center of the oven a position could be determined at which both sides of the sample holder were heated at equal rates. Thus copper wire extensions

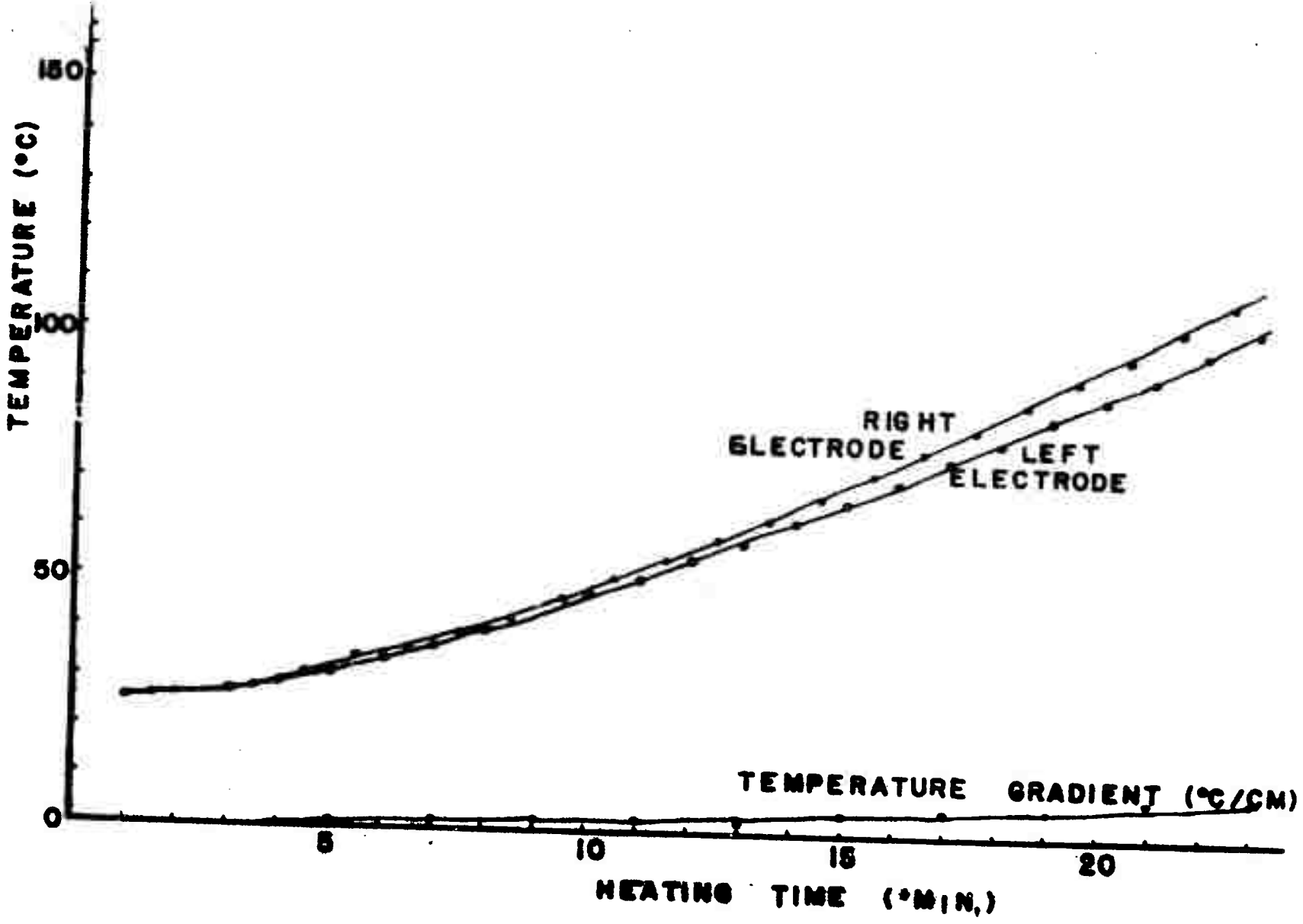

Figure III-4. Temperature gradient measurement on Lucite 1.0 cm thick.

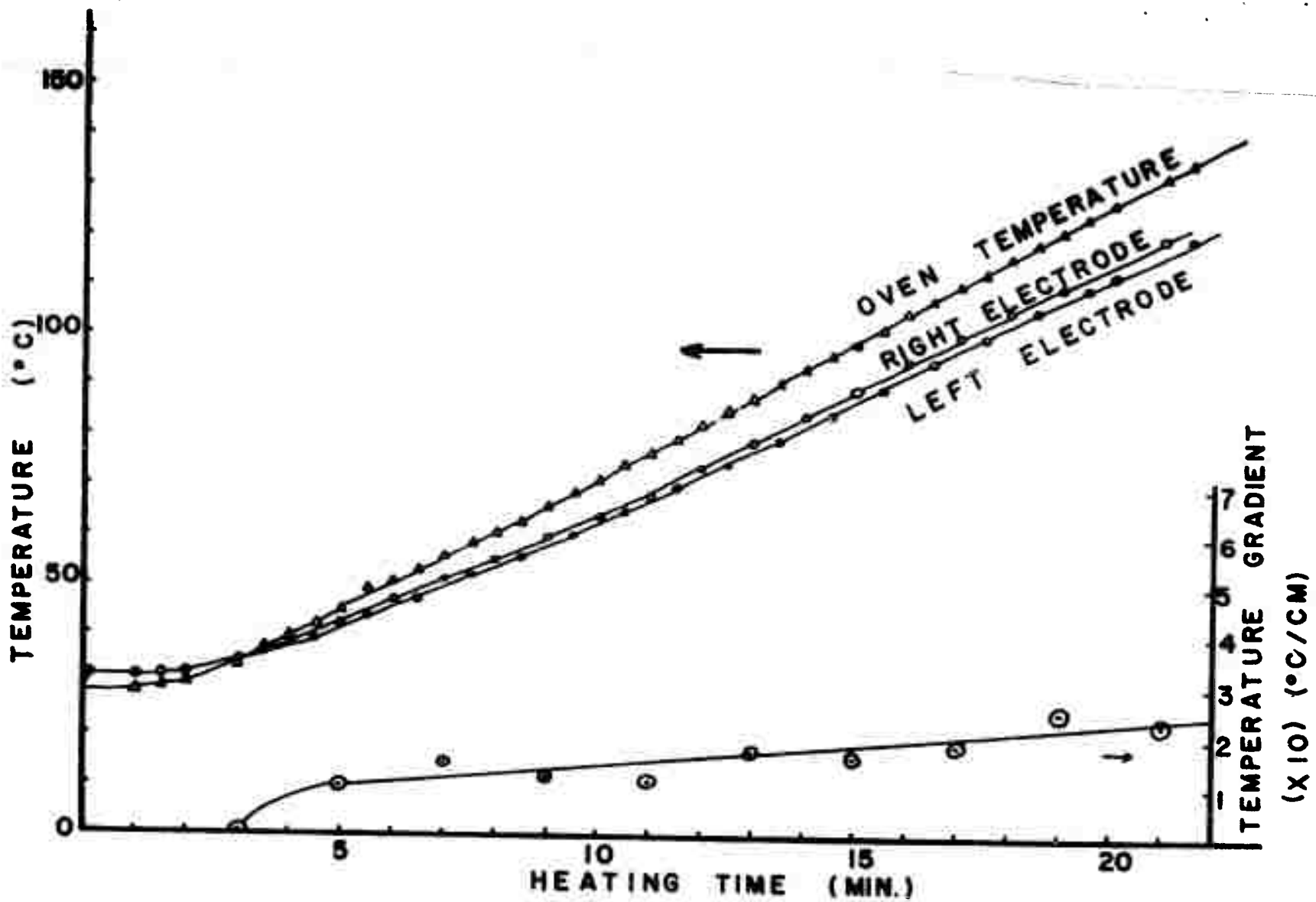

Figure III-5. Temperature gradient measurement on Lucite 0.1 cm thick.

to the input plug and electrometer ground were necessary to prevent any appreciable conduction of heat away from the sample holder. A plot of the temperature difference of the sample electrodes when heated in this configuration is shown in Figure III-6.

e. Polymerization Techniques

Inhibitor free methylmethacrylate (MMA) monomer, 99.95% pure, was obtained from the Rohm and Haas Company. Polymerization of this monomer occurs by a free radical process. Unreacted monomer molecules add to monomer free radicals to form the polymer chain. The process is known as addition polymerization.[5] If the monomer free radicals are the result of the presence of a chemical initiator (I) the process can be represented by the following reactions:

$$I \longrightarrow 2R^{\bullet}$$

$$R^{\bullet} + M \longrightarrow M_1^{\bullet}$$

$$M_1^{\bullet} + M \longrightarrow M_2^{\bullet}$$

$$M_x^{\bullet} + M \longrightarrow M_{x+1}^{\bullet}$$

The chain continues to propagate until the monomer molecules become depleted, the terminal free radicals combine with other species, or the viscosity increases until monomer molecules can no longer move to the end of the chains.

Polymerization of monomeric MMA can be initiated by ultraviolet light, traces of oxygen or peroxides, elevation of temperature, or by the addition of certain chemical initiators.[6] Polymerization with ultraviolet light (photopolymerization) was accomplished in a Rayonet U. V. Reactor. The light source consists of sixteen 3500 Å mercury vapor fluorescent lamps arranged

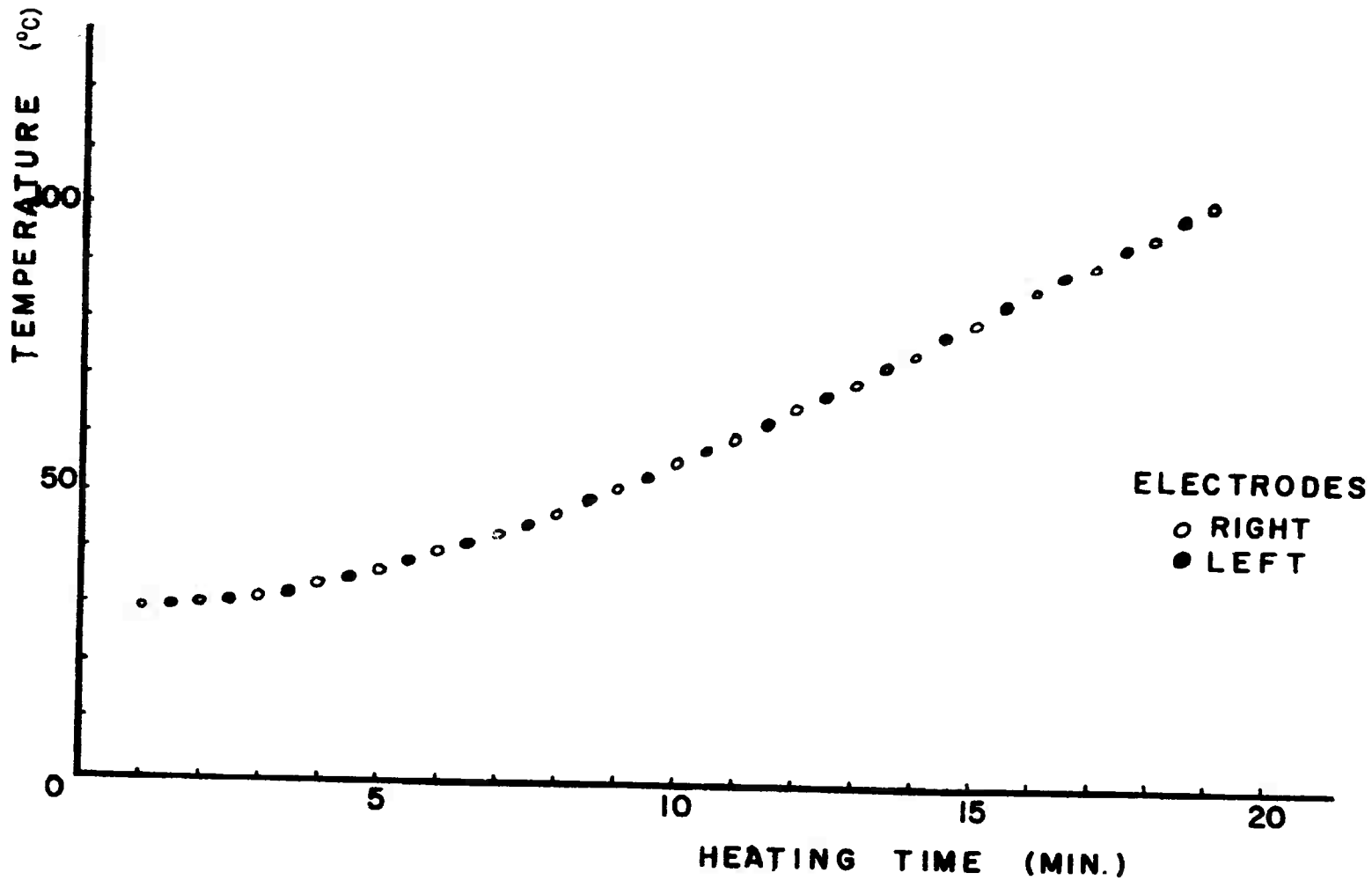

Figure III-6. Zero temperature gradient measurement.

in a cylindrical configuration with a combined intensity given by the manufacturer of 1.5 to 5 X 10^{16} photons/sec/cm^3. The ultraviolet irradiation was carried out in cylindrical pyrex glass tubes. A 24-hour exposure was necessary to obtain a hard polymer.

Thermal polymerization of MMA required 48 hours at a temperature of 90°C. Riddle[7] recommends a variation of temperature in a cycle ranging from 40 to 110°C in order to control the polymerization process during its accelerated stages. This method is now being explored.

The effect of oxygen on the polymerization of MMA has been investigated[8] and found to have a definite inhibiting effect on the polymerization. It has been shown that a low molecular weight polymeric peroxide is formed with MMA which has the following probable structure.[9]

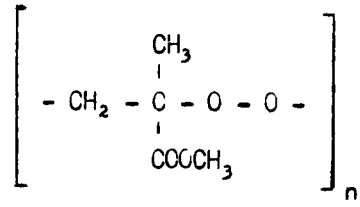

polyperoxide

This polyperoxide then decomposes to give formaldehyde and methylpyruvate. In addition the oxygen probably acts as a chain terminator in the early stages of polymerization. The polymeric peroxide can initiate polymerization which may sometimes be extremely rapid.[7]

Oxygen was removed from the monomer prior to polymerization by the freeze - pump - thaw method for all samples reported herein. It has been found that the monomer can be equally effectively deoxygenated by purging for 15 minutes with dry nitrogen. All future samples will be deoxygenated by purging since it is more rapid than the freeze - pump - thaw method.

As mentioned previously benzoyl peroxide is the most commonly used chemical initiator in the commercial polymerization of MMA. A tertiary amine activator, such as N,N-dimethylaniline, N,N-dimethyl-p-toluidine or trihexylamine is sometimes used with benzoyl peroxide to speed up the reaction at room temperature.[7]

All data on synthesized polymers presented in this report were obtained from photopolymerized samples unless the material added was benzoyl peroxide which itself served to catalyze the polymerization. Thermal polymerization methods arepresently being explored.

f. Sample Irradiation

All samples were irradiated in a 2900 curie U. S. Nuclear GR-9 Co-60 Irradiator at a dose rate of approximately .5 Mrad/hr. The source is arranged in a cylindrical configuration around the 4" diameter sample chamber to provide approximately isotropic irradiation. Samples were supported by one of the metal tabs attached to the sample electrodes, and were positioned in the center of the irradiation chamber to assure uniform exposure. The ambient temperature of the source is about 35°C.

3. RESULTS

a. Current Measurement

A typical current vs. time plot of a 1 cm thick Lucite sample is shown in Figure III-7. The sample was heated linearly at a rate of 6°C/min after a dose of 0.5 Mrad. The curve is approximately symmetrical with a peak of 5.9 picoamps (pa) at 65°C. Figure III-8 is a similar plot for a PVC sample measured under the same conditions. The peak current is 31 pa and occurs at a temperature of 86°C. A second heating of each sample resulted in no measurable current.

All temperatures mentioned were measured at the higher temperature sample electrode. For temperatures above 90°C in Lucite electronic noise was observed on the recorder. This temperature corresponds to the glass transition temperature (Tg) for PMMA. The filtering circuit mentioned previously allowed the measurement of the thermoelectric current in the presence of noise to a temperature of 120°C. Heating samples above 150°C caused gas bubbles to form in the material and caused the samples to swell.

Integration of the current vs. time curves does not yield values equal to the actual total charge released in the sample but rather gives values proportional to the total charge release. This is because each charge carrier released moves only a fraction of the distance between the electrodes before it is neutralized, and therefore contributes only a fraction of a charge carrier to the total current measured in the external circuit. Integration of all curves to obtain normalized values proportional to the total charge released in a sample were carried out to a temperature of 120°C.

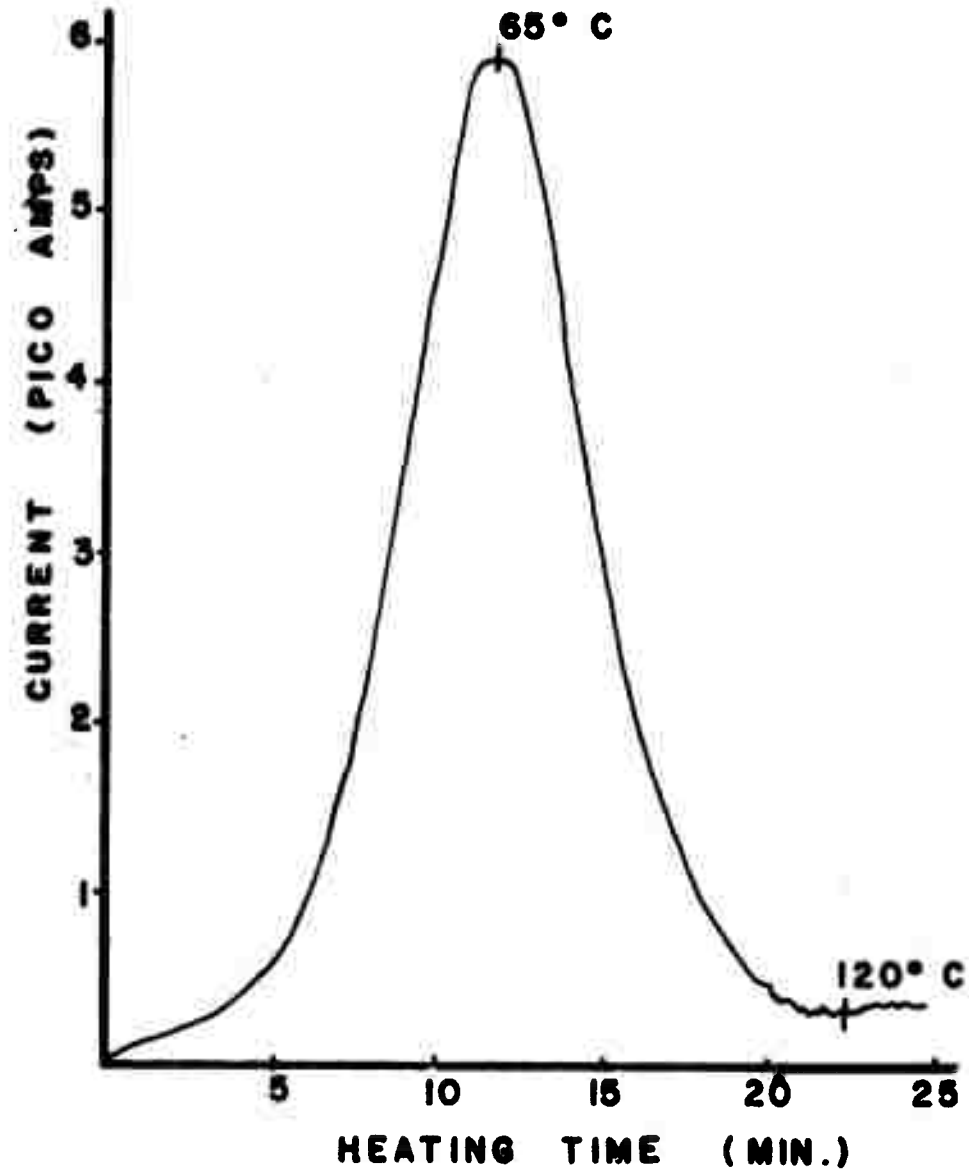

Figure III-7. Thermoelectric current plot for Lucite.

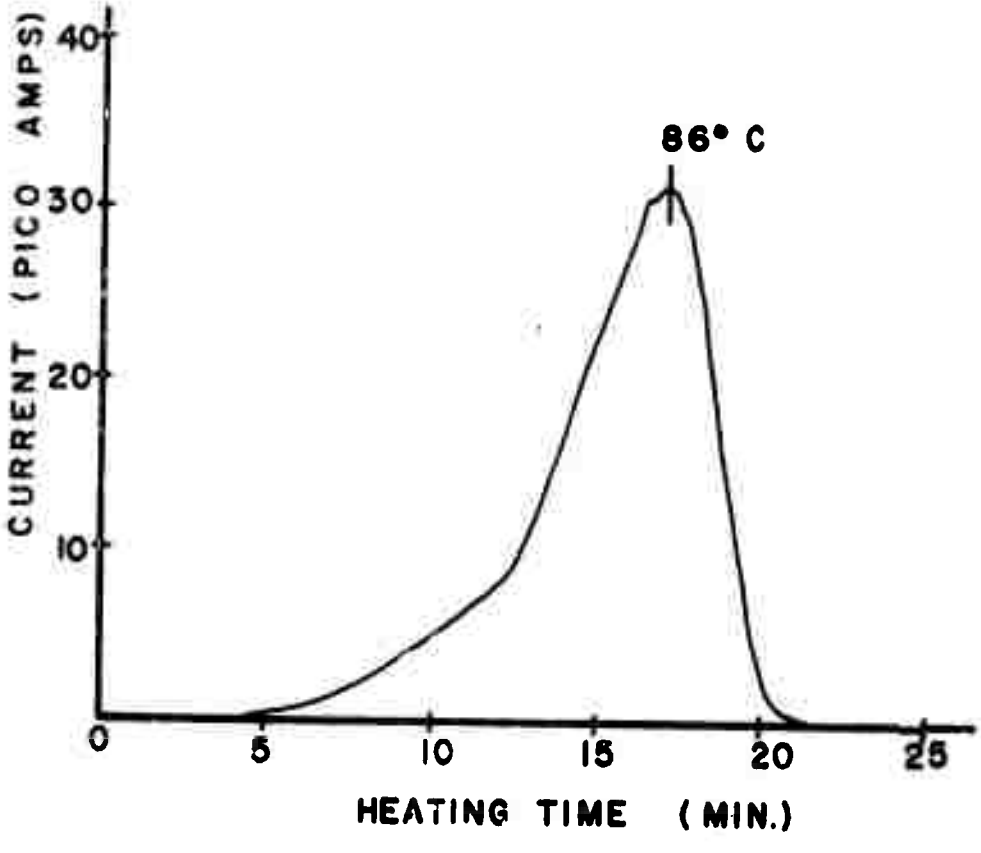

Figure III-8. Thermoelectric current plot for PVC. The asymmetry is often observed and its origin is unknown.

b. Dose Effects

Samples of Lucite 1 cm thick were given doses from 0.12 Mrad to 20 Mrad. These samples were then heated linearly at a rate of 6°C/min while the currents were measured. Results of the measurements are shown in Table III-I and Figure III-9. The total charge released from the sample increases with dose to about 1 Mrad. It then appears to remain relatively constant to at least a dose of 20 Mrad. This constant value of normalized total charge released suggests a saturation of trapped charge carriers in the material at quite low doses.

c. Effect of Heating Rate

A change in the rate of heating a sample primarily changes the temperature gradient imposed on the sample. The temperature gradient influences the movement of charge carriers predominantly in one direction and therefore the recombination of charge carriers of opposite sign. Table III-II contains the important parameters of thermoelectric current peaks measured at heating rates from 2°C/min to 12°C/min. The variation in normalized total charge with heating rate is shown graphically in Figure III-10 while Figure III-11 illustrates the relation of heating rate to peak current. Both parameters increase linearly with heating rate although the effect on peak current was much greater. All samples were 1 cm thick and were given a dose of 0.5 Mrad.

d. Zero Temperature Gradient

A position in the oven had been determined as described previously (Figure III-6) at which a sample could be heated with a very small temperature

Table III-I: Effect of Absorbed Dose on Thermal Induced Charge Release in Lucite

Heating Rate: 6°C/min. Samples 1 cm Thick

Exposure Time	Total Dose	Peak Current	Temperature at Peak	Normalized Total Charge[a]
Hours	Mrad	picoamps.	°C	arbitrary units
0.25	0.12	3.9	65	119.9
0.5	0.25	4.8	65	127.5
1	0.5	5.9	65	168.0
2	1.0	6.2	62	155.6
10.25[b]	5.1	5.8	66	158.1
		0.45	121	
20[b]	10	5.7	66	161.3
		0.65	120	
40[b]	20	5.6	62	158.1
		1.3	102	

[a] Curves integrated to 120°C

[b] Two current peaks observed

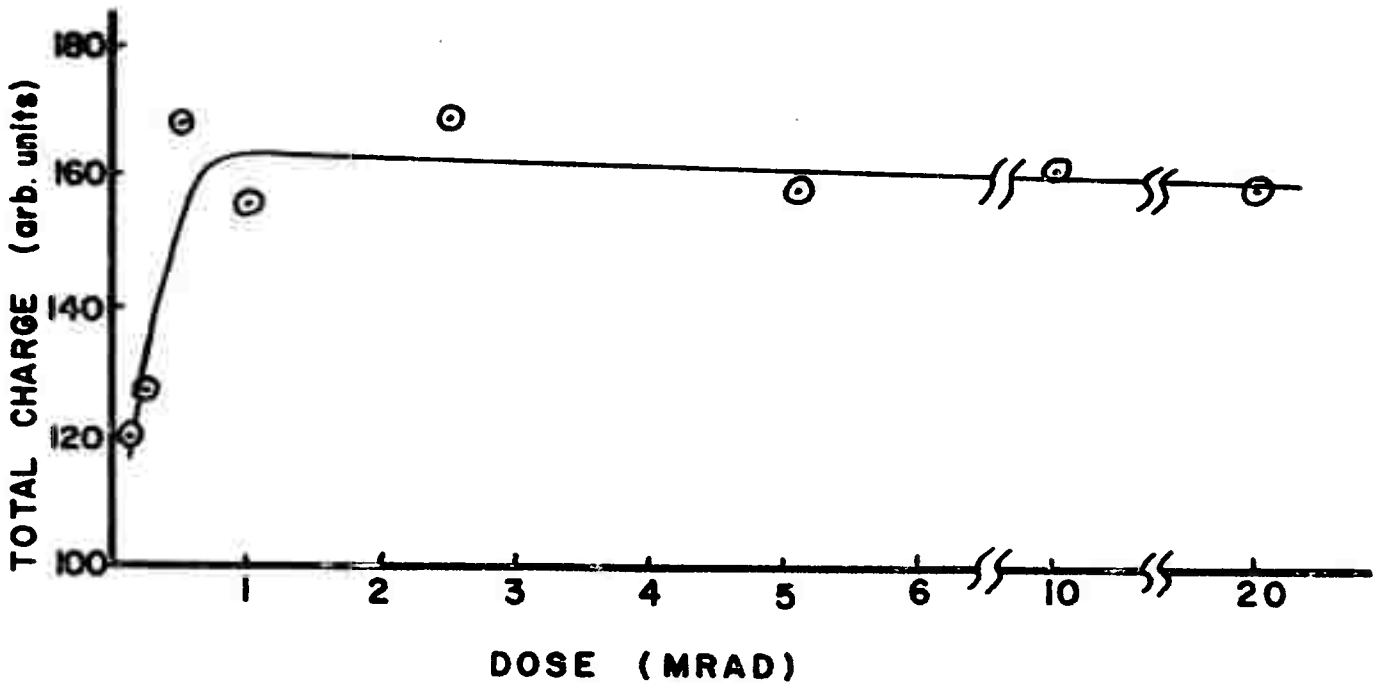

Figure III-9. Thermal induced charge release vs. absorbed dose.

Table III-II: Effect of Heating Rate on Thermal Induced Charge Release in Lucite

Absorbed Dose: 0.5 Mrad — Samples 1 cm Thick

Heating Rate	Peak Current	Temperature at Peak	Normalized Total Charge[a]
°C/min	picoamps	°C	arbitrary units
2	1.9	53	108.0
4	2.8	59	100.5
6	5.9	65	168.0
8	6.5	65	141.6
10	7.6	69	155.2
12	10.4	68	193.8

[a] Curves integrated to 120°C

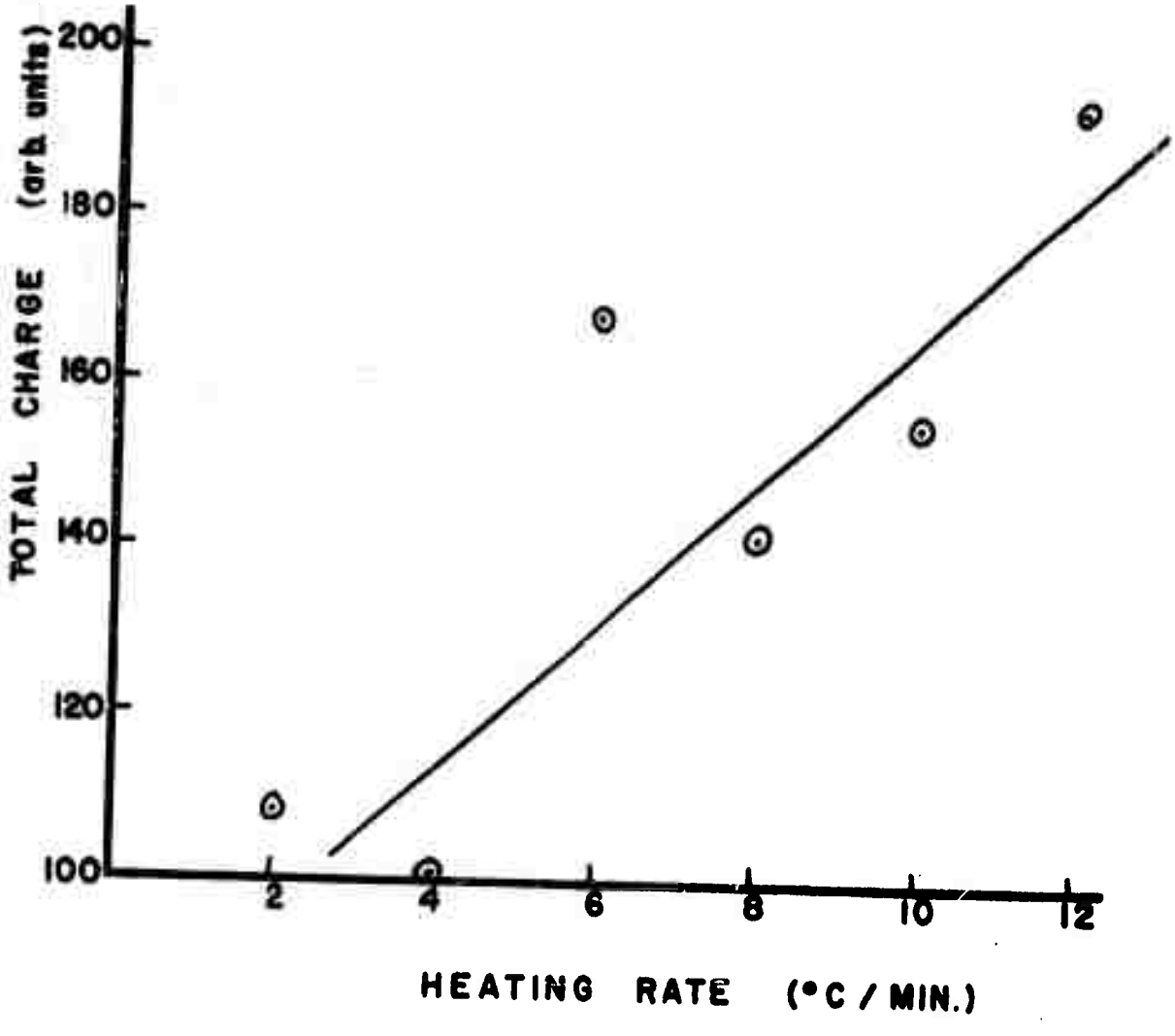

Figure III-10. Effect of heating rate on normalized total charge.

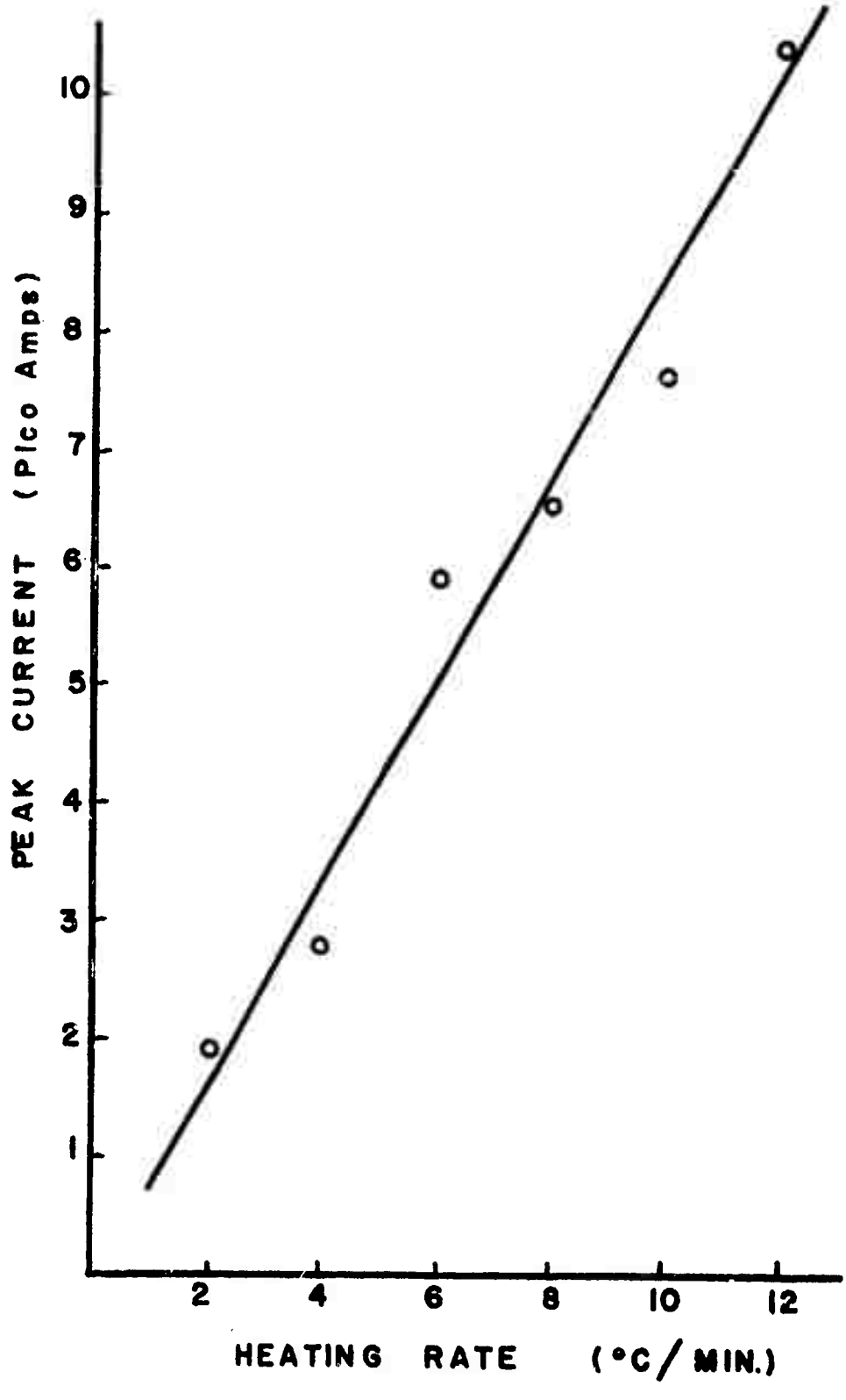

Figure III-11. Effect of heating rate on peak current.

difference between the sample electrodes. In order to determine the importance of the temperature gradient on the current measurements, an experiment was performed with a sample in this position. The result of this heating is shown in Figure III-12. The Lucite sample was 1 cm thick and had received 0.5 Mrad of gamma irradiation. The oven was heated linearly at a rate of $6^{o}C/min$. Both the peak height and area under the curve were reduced by factors of approximately 10 and 20, respectively, compared with samples measured under similar conditions but in the normal sample position. This is evidence that a temperature gradient is essential to the measurement of the observed thermoelectric currents.

e. Successive Irradiations on the Same Sample

All measurements made in this investigation were performed on samples with no known previous irradiation history with the exception of those reported in this section. Table III-III gives the parameters for two different Lucite samples irradiated and measured three successive times. Similar measurements were made on two PVC samples, Table III-IV. The radiation was expected to produce products which might act as additional or deeper trapping sites. An increase in normalized total charge is apparent in most samples.

f. Variations of Sample Thickness

The results of measuring the thermoelectric current in samples of different thickness are shown in Figures III-13 and III-14. In Figure III-13 the current vs temperature plots for selected samples between 1.0 and 0.17 cm thick are superimposed and the same curves for samples between 0.10

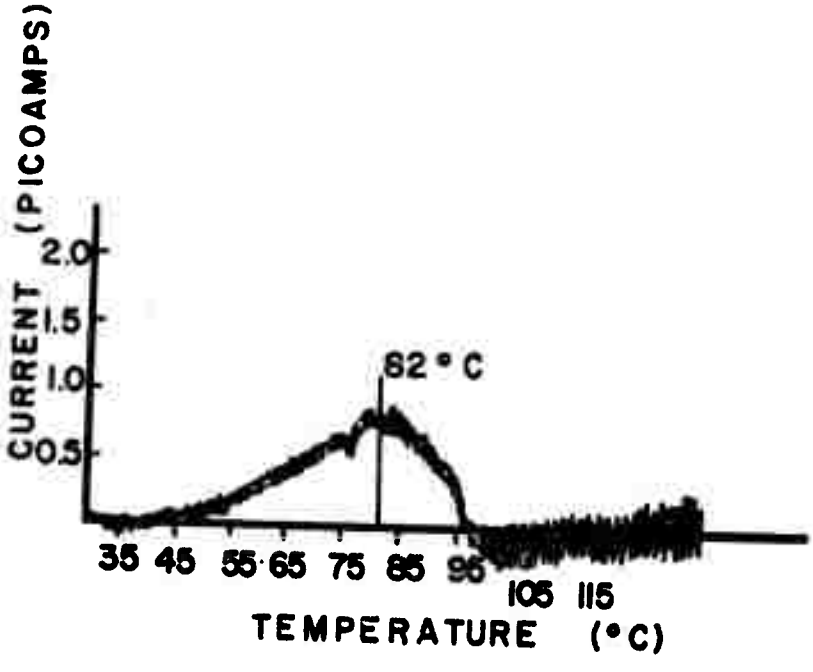

Figure III-12. Thermoelectric current plot for zero temperature gradient.

Table III-III: Successive Irradiations and Measurements of Thermoelectric Currents in Lucite

Absorbed Dose: 0.5 Mrad Heating Rate: 6°C/min.

Trial no.	Peak Current	Temperature of Peak	Normalized Total Charge
	picoamps	°C	arbitrary units
Sample no. 229			
1	5.5	85	178.9
2	5.7	86	180.9
3	5.5	84	192.1
Sample no. 230			
1	4.8	86	160.8
2	5.7	86	180.9
3	5.6	83	210.5

Table III-IV: Successive Irradiation and Measurement of Thermoelectric Currents in Polyvinyl Chloride

Absorbed Dose: 0.5 Mrad Heating Rate: 6°C/min.

Trial no.	Peak Current	Temperature of Peak	Normalized Total Charge
	picoamps	°C	arbitrary units
Sample no. 231			
1	31	85	67.4
2	32	85	74.6
3	38	86	76.3
4	void	void	void
5	47	82	87.8
6	48	82	85.4
Sample no. 232			
1	31	86	67.5
2	32	84	74.5
3	35	86	81.5

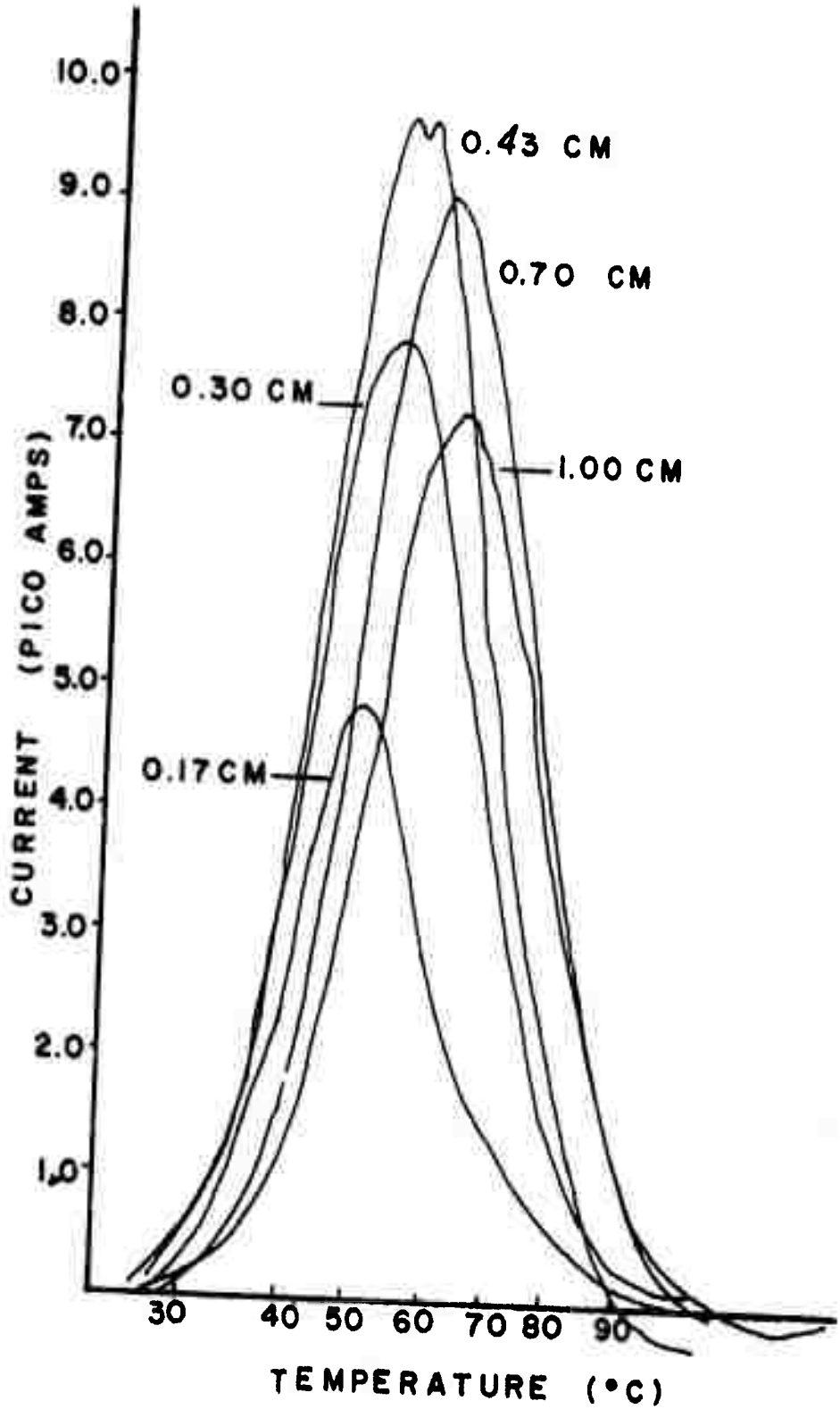

Figure III-13. Current profiles for sample thicknesses from 1.0 cm to 0.17 cm.

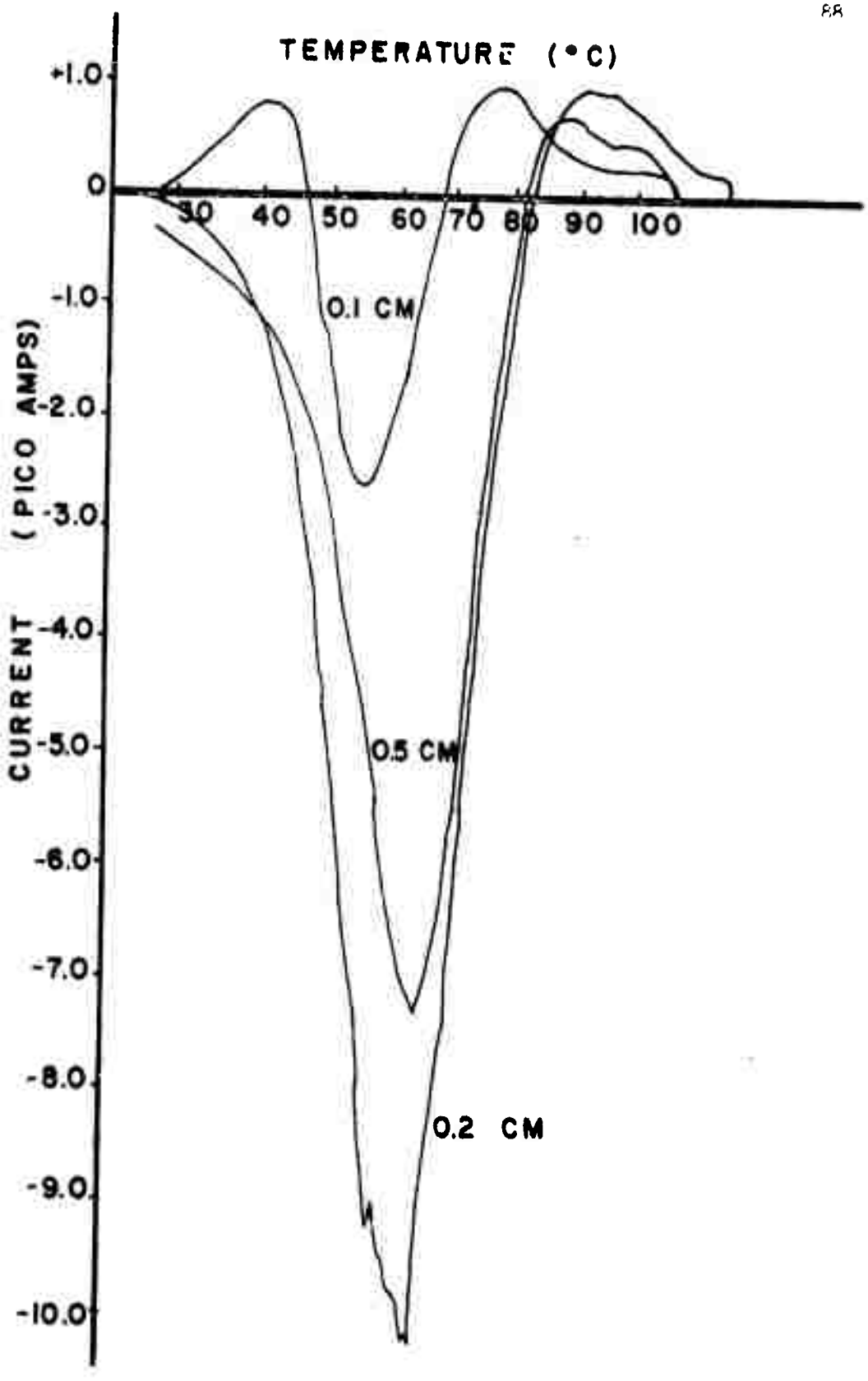

Figure III-14. Current profiles for sample thicknesses from 0.10 cm to 0.02 cm.

and 0.02 cm thick are illustrated in Figure III-14. All measurements were made after a dose of 0.5 Mrad and for a linear heating rate of 6°C/min. Integration of the current vs temperature plots was performed to obtain relative values proportional to the net charge released in the sample. The net area was obtained by subtracting the area under the positive and negative current peaks. These values were plotted against sample thickness in Figure III-15. Examination of this figure indicates a maximum net charge release for a sample thickness of approximately 0.4 cm and a zero net charge release for a thickness of about 0.09 cm.

g. Decay Studies

A study was made of the decay of the total charge released in Lucite at various temperatures. Samples 1.0 cm thick were given doses of 0.5 Mrad and after decay at various constant temperatures, they were measured at a linear heating rate of 6°C/min. Table III-V shows the results of these measurements.

The normalized total charge vs decay time for Lucite samples is shown in semilog plots in Figure III-16 for selected temperatures from 0°C to 50°C. All the decay curves appear to contain two components, a rapid initial decay and a slower long term decay.

Decay constants were obtained from the slope of linear portions of the Lucite decay curves and were plotted on semilog paper against the inverse of the absolute temperature to obtain an Arrhenius plot, Figure III-17. The slope of this line is equal to the activation energy (Ea) divided by the universal gas constant (R). For Lucite the activation energy was calculated to be 20.7 kcal/mole (0.9 ev). Preliminary decay measurements on PVC show that trapped charges are much more stable in it. Detailed decay studies on PVC are in progress.

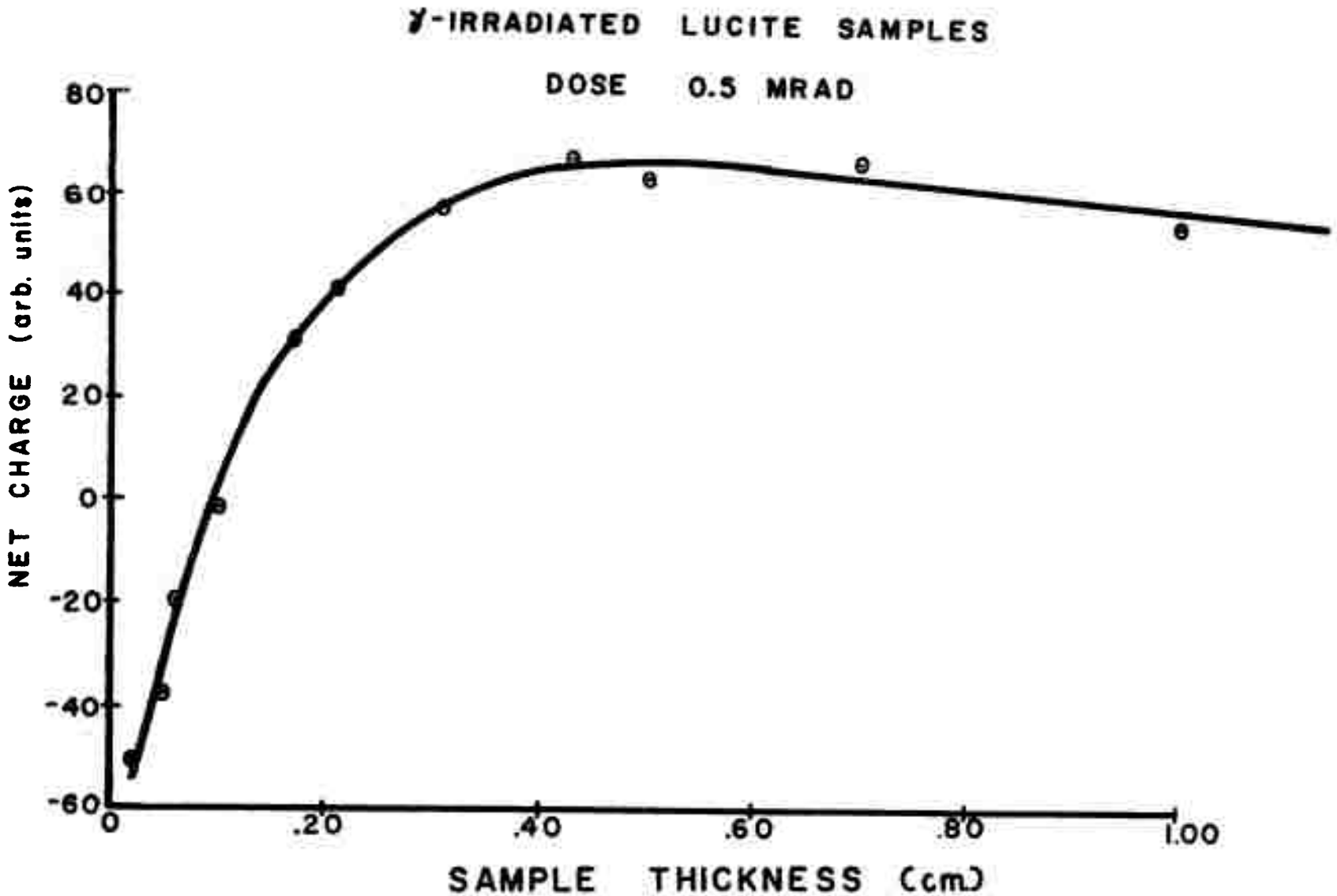

Figure III-15. Net current vs. sample thickness in Lucite.

Table III-V: Decay of Trapped Charge Carriers in Lucite at Various Temperatures

Samples 1 cm Thick

Absorbed Dose: 0.5 Mrad **Heating Rate 6°C/min.**

Decay Time	Peak Current	Temperature of Peak	Normalized Total Charge
hours	picoamps	°C	arbitrary units
Temperature 0°C			
5	4.7	88	152.1
10	4.9	88	153.9
20	4.9	86	150.6
40	5.2	89	171.7
168	3.9	88	—
336	3.7	90	112.3
Temperature 15°C			
5	4.6	88	135.4
10	4.0	88	121.0
15	3.5	89	106.0
20	3.1	88	97.0
25	3.2	88	88.3
Temperature 25°C			
1	3.9	88	138.0
2.5	3.6	89	109.9
5	2.9	95	81.5
10	2.1	100	59.6
15	1.7	100	54.2
20	1.4	101	40.4
25	1.2	104	36.6
27	1.15	105	35.4
Temperature 35°C			
2.5	2.0	98	62.2
5.0	1.5	100	50.6
7.5	0.8	105	25.7
10	0.7	106	19.0
Temperature 50°C			
1.0	1.2	106	29.3
1.5	0.5	112.5	18.3
2.0	0.34	121	13.6
2.5	0.37	119	12.3
3.0	0.35	122	8.6

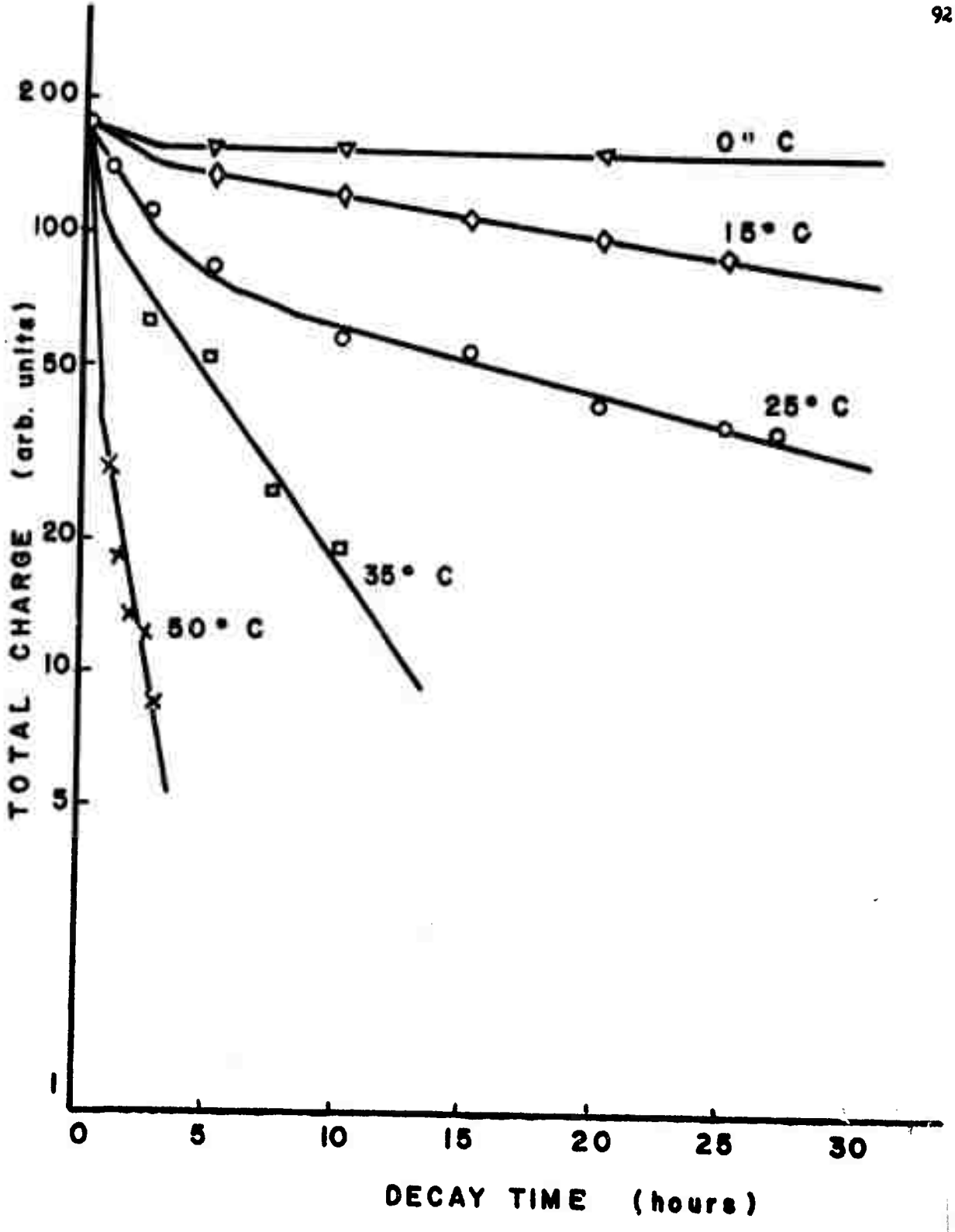

Figure III-16. Decay of thermoelectric currents in Lucite samples.

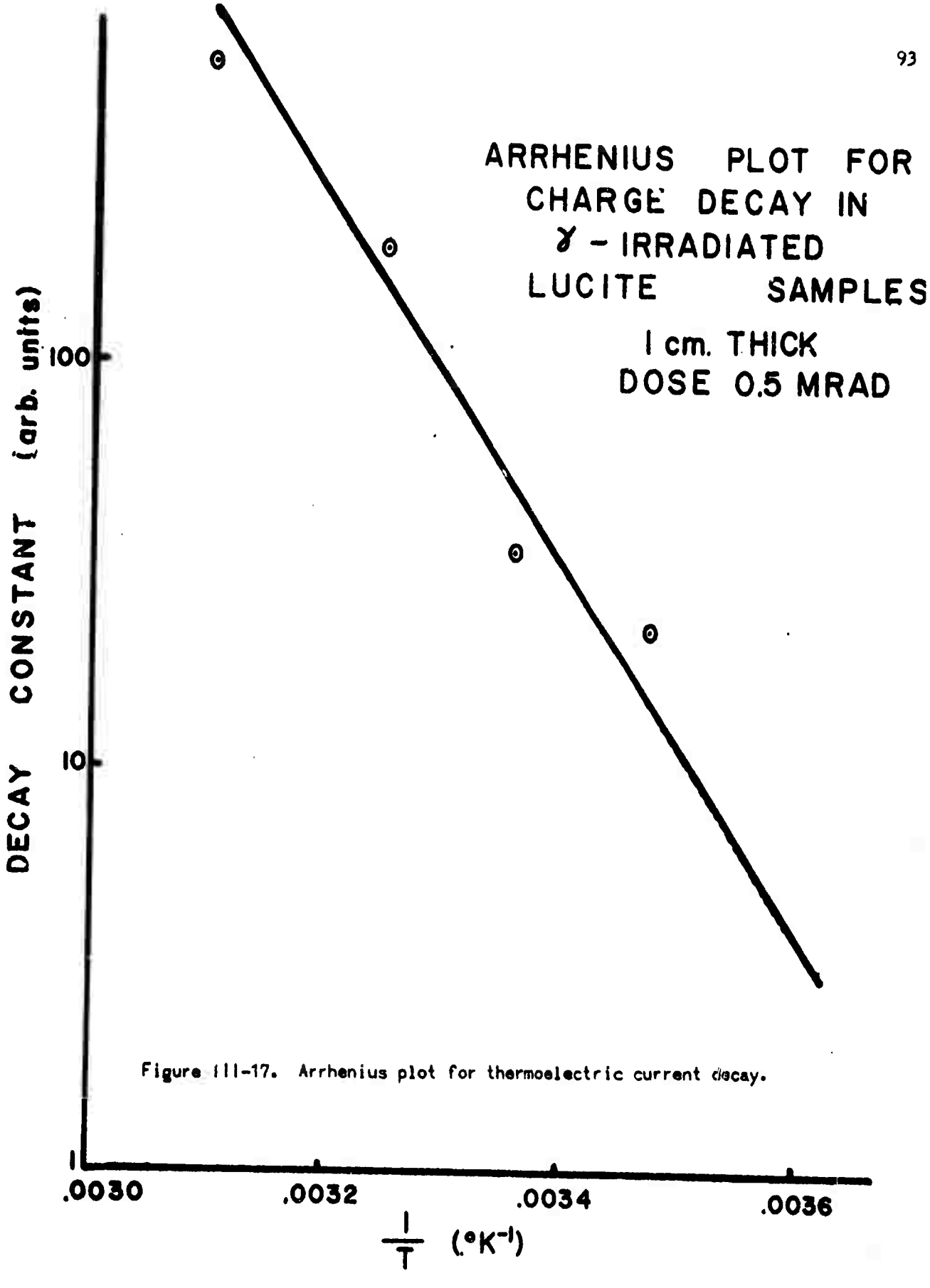

Figure III-17. Arrhenius plot for thermoelectric current decay.

h. Effect of Additives

Pure PMMA was photopolymerized with and without various selected additives as described previously. Samples were prepared from these synthesized materials. The samples were given a dose of 0.5 Mrad and subsequently were heated at a linear rate of 6°C/min for current measurement. The results of this study are given in Table III-VI. Pure PMMA with no additives produces a very small thermoelectric current while the presence of small concentrations of electron traps like carbon tetrachloride or benzoyl peroxide increase this current by a factor of at least 10. Similar concentrations of benzene and chlorobenzene do not increase the current over that in pure PMMA. The hole trap, 2-methylpentene-1, causes a twofold increase in the current for one run; further experiments are necessary to ascertain if this increase is significant. The relatively large current from PVC samples is not unexpected in view of the results of CCl_4 as an additive.

A measurement on irradiated polyethylene resulted in a negligible thermoelectric current. Samples of Teflon and triethyleneglycoldimethacrylate (Tedma) also produced nearly zero thermoelectric currents after irradiation and heating.

Table III-VI: Thermoelectric Currents from Synthesized Polymers

Material	Additive	Sample Thickness (cm)	Peak Current (picoamps)
PMMA	None		
Sample 1		1.0	0.40
Sample 2		0.4	0.33
PMMA	Benzoyl Peroxide (.41 mole %)		
Sample 1		1.0	3.6
Sample 2		0.4	4.3
PMMA	(1 mole %)		
Sample 1		0.4	5.6
Sample 2		0.4	4.6
Sample 3		0.4	4.5
PMMA	Benzene (1 mole %)	0.4	0.45
PMMA	Chlorobenzene (1 mole %)		
Sample 1		0.4	0.53
Sample 2		0.4	0.33
PMMA	2-Methylpentene-1 (1 mole %)	0.4	1.1
Poly Vinyl Chloride (Chloroethylene)	(Commercial)		
Sample 1		1.0	32.5
Sample 2		1.0	33.6
Sample 3		0.4	56.0
Sample 4		0.4	50.2

4. DISCUSSION

The discussion herein is somewhat speculative since the data is only partially complete. Our present ideas are briefly summarized but are subject to modification based on future results.

a. Model of Thermoelectric Current Generation

The results on the synthesized polymers in Table III-VI are quite revealing. Pure PMMA with no additive exhibits a very small current. Few charges appear to be trapped in it during irradiation at 35°C. Thus either or both positive and negative charges are mobile and cause recombination.

If CCl_4 or benzoyl peroxide are added to PMMA the observed current increases by 10 - 20 times over that with no additive. CCl_4 is well known to react with electrons by dissociative electron attachment in solid organic matrices.[4] It seems likely that benzoyl peroxide can act in a similar manner because of its weak O-O bonds and the electron affinity of oxygen. Alternatively, it is probable that peroxide and oxide radicals from benzoyl peroxide are produced during polymerization and can act as electron traps. It should further be pointed out that electron traps produced by dissociative attachment or by oxygen containing radicals are quite thermally stable and may well be stable above room temperature in a polymer matrix. That is "deep" traps are produced.

If deep electron traps are provided charge is stored and the thermally generated current increases. This suggests that at room temperature in pure PMMA, radiation-produced electrons are mobile and recombine with

trapped holes during irradiation. If the holes were also mobile in the presence of an electron trap, recombination could still occur which is contrary to our observations. This tentative conclusion is supported by the addition of 2-methylpentene-1 (2MP-1) to PMMA. In solid organic matrices 2MP-1 is an excellent hole trap and a relatively poor electron trap.[4] PMMA doped with 2MP-1 only shows a twofold increase in the thermally generated current. A much larger increase (for example 10-fold) would be expected if the holes were mobile and the electrons were trapped in pure PMMA. The twofold increase if verified in additional samples is more likely due to the weak electron trapping nature of 2MP-1.

Both benzene and chlorobenzene act as poor electron and hole traps in solid organic matrices.[4] That they cause no increased current in PMMA is consistent with the above results.

Polyvinyl chloride shows a very large current. It is a polyalkyl chloride and can itself react with electrons by dissociative electron attachment. Alkyl chlorides readily show this reaction in the solid phase.[10] In contrast, teflon shows negligible current. The C-F bond is strong enough to preclude dissociate electron attachment. (This is verified by the poor response of linear saturated fluorocarbons to an electron capture detector in a gas chromatograph.) Consequently, the results on PVC and on teflon are consistent with those for doped PMMA.

Commercial PMMA (Lucite) is thermally polymerized with benzoyl peroxide; thus it should be similar to PMMA doped with benzoyl peroxide. This has been verified; Lucite shows currents of similar magnitude to those of PMMA doped with benzoyl peroxide. Thus Lucite is convenient to work with since it has a built-in electron trap. It should be remembered though that the

currents observed in Lucite are characteristic of added electron traps and not of pure PMMA itself.

The observation of thermally generated currents indicates that one or both charge carriers are mobilized by thermal stimulation. It should be noted that the peak current occurs near 65°C which is well below the glass transition temperature of PMMA at 90°C.[5] Thus the temperature of detrapping seems to be characteristic of the trapping site rather than of the unirradiated polymer. It might be expected that if the electrons were thermally detrapped that the temperature at which the peak current occurs should depend on the type of electron trap. However, the temperature of the peak current is the same in CCl_4 and benzoyl peroxide doped PMMA. This result suggests that trapped holes are mobilized by the thermal excitation. Hole mobility is also suggested by the polarity of the colder electrode as discussed below.

It should be stressed that the currents studied thus far are thermoelectric; they require a temperature gradient for their generation. Therefore, the polarity of the current can give information about the sign of the majority charge carrier. The existence of a temperature gradient means that there is a net propagation of lattice vibration waves or phonons from the hot to the cold electrode. The phonons interact with the mobile charge carriers and cause the most mobile charge carrier to drift in the direction of the phonons. Therefore the sign of the cold electrode corresponds to the majority or most mobile charge carrier.[11,12] In all measurements on samples thicker than 0.10 cm the cold electrode has been positive with respect to ground. This indicates that holes are the mobile species and supports the suggestion of hole mobility based on the additive results.

b. Stability of Trapped Charge

The decay curves in Figure III-16 can be divided into two sections. The initial curved section is formally characterized by a reaction order greater than one while the straight line section corresponds to first order decay. Similarly shaped decay curves have been observed for radiation-produced hydrogen atoms in solids.[13] The initial curved part of the decay curve can arise from a superposition of several first order decay curves with different activation energies. This suggests that a small number of charges are trapped in a distribution of shallow potential wells. Such shallow traps may, in fact, account for the small currents observed in pure PMMA. The majority of the charges are trapped in deeper potential wells. These sites appear to be characterized by a single trap depth or a relatively narrow distribution of trap depths because a good Arrhenius plot is obtained. First order decay corresponds to release from the traps rather than to charge recombination between positive and negative centers.

The decay constants derived from the linear sections of the decay curves show a good fit to an Arrhenius plot (Figure III-17). The apparent activation energy is 20.7 kcal/mole (0.9 ev) in Lucite which is equivalent to PMMA doped with benzoyl peroxide. According to the model of thermo-electric currents in Lucite postulated above this activation energy is associated with the hole traps. Experiments are in progress on doped PMMA to determine whether the activation energy is independent of the type of added electron trap.

The mere observation of a large activation energy indicates that tunneling is not the mobility mechanism. At present a thermally activated hopping mechanism seems likely for hole mobility. It is of interest to obtain more direct information on the mobility mechanism.

c. Sample Thickness Effects

Two factors could affect the change in thermoelectric current with decreasing sample thickness, the temperature gradient and the trapped charge distribution. The temperature gradient increases with a decrease in sample thickness. This is apparent in a comparison of temperature gradients in Lucite samples 1.0 cm thick and 0.10 cm thick (Figures III-4 and III-5). This may contribute to the increase in current when the sample thickness is decreased from 1.0 cm to 0.4 cm. However it does not explain the change in the polarity of the current observed during measurement of samples between 0.10 cm and 0.02 cm thick (Figure III-14).

The charge distribution will be fairly uniform throughout the interior volume of the thicker samples. At the surfaces of the sample the distribution will not be uniform because of the build-up of secondary electron density as the photon flux passes from a lower to a higher atomic number medium (i.e., air to polymer). In thicker samples the effect of the nonuniform charge distribution at the surfaces is small compared to the charge distribution throughout the volume. As the sample thickness is decreased the surface effects are accentuated. More work is necessary before the relative importance of these contributing factors can be ascertained.

d. Dose Saturation of Traps

Figure III-9 indicates that the normalized total charge saturates after a dose of 1.2 Mrad. This presumably is the dose at which all available traps are filled or at which back reactions are important. It has been postulated here that added impurities provide the trapping sites.

Another possibility is that free radicals formed in the polymerization process and created by main chain scission during irradiation could participate in charge trapping. Ohnishi and Nitta[14] have measured the free radical concentrations in PMMA after Co-60 irradiation. They report that the radical concentration saturates at a dose of 7 Mrad and is a linearly increasing function of dose to about 2.5 Mrad. Since dose saturation of trapped charge occurs at much lower doses, this is indirect evidence that free radicals do not provide the predominant trapping sites in PMMA. The absence of large currents in pure PMMA also substantiates this conclusion.

5. REFERENCES

1. F. C. Hardtke, J. Chem. Phys., 42, 3000 (1965); Phys. Rev. Letters, 9, 339 (1962).

2. B. Gross, Phys. Rev., 110, 337 (1958).

3. J. E. Barnes, M.Sc. Thesis, University of Kansas, 1965.

4. W. H. Hamill, "Radical Ions," Eds. E. T. Kaiser and L. Kevan, Wiley Interscience, New York, 1968, Chapter 9.

5. P. Flory, "Principles of Polymer Chemistry," Cornell University Press, Ithaca, New York, 1953.

6. W. J. Roff, "Fibres, Plastics and Rubbers," Academic Press, New York, 1956, pp. 195-201.

7. E. H. Riddle, "Monomeric Acrylate Esters," Reinhold, New York, 1954, p. 36.

8. C. E. Schildknecht, "Vinyl and Related Polymers," Wiley, New York, 1952, pp. 186-191.

9. C. E. Barnes, R. M. Elofson and G. D. Jones, J. Am. Chem. Soc., 72, 210 (1950).

10. R. F. Claridge and J. E. Willard, J. Am. Chem. Soc., 87, 4992 (1965).

11. D. K. C. MacDonald, "Thermoelectricity: An Introduction to the Principles," Wiley, New York, 1962, pp. 19-20.

12. F. Gutman and L. Lawrence, "Organic Semiconductors," Wiley, New York, 1967, pp. 72-78.

13. D. Schulte-Frohlinde, private communication (1967).

14. S. Ohnishi and I. Nitta, J. Poly. Sci., 38, 451 (1959).

Unclassified
Security Classification

DOCUMENT CONTROL DATA - R&D

(Security classification of title, body of abstract and indexing annotation must be entered when the overall report is classified)

1. ORIGINATING ACTIVITY (Corporate author)
Department of Chemistry
University of Kansas
Lawrence, Kansas 66044

2a. REPORT SECURITY CLASSIFICATION
Unclassified

2b. GROUP

3. REPORT TITLE

Structure and Reactivity of Energetic Chemical Species

4. DESCRIPTIVE NOTES (Type of report and inclusive dates)
Annual Summary Report (1 November 1966 to 31 October 1967)

5. AUTHOR(S) (Last name, first name, initial)
Kevan, Larry
Harmony, Marlin
Christoffersen, Ralph
Barnes, James

6. REPORT DATE
December, 1967

7a. TOTAL NO. OF PAGES
102

7b. NO. OF REFS
52

8a. CONTRACT OR GRANT NO.
F04611-67C-0032

b. PROJECT NO.

c.

d.

9a. ORIGINATOR'S REPORT NUMBER(S)

9b. OTHER REPORT NO(S) (Any other numbers that may be assigned this report)

10. AVAILABILITY/LIMITATION NOTICES
This document is subject to special export controls and each transmittal to foreign governments or foreign nationals may be made only with prior approval of AFRPL (RPPR-STINFO), Edwards, California 93523.

11. SUPPLEMENTARY NOTES

12. SPONSORING MILITARY ACTIVITY
Rocket Propulsion Laboratory
Edwards Air Force Base, California

13. ABSTRACT

Energetic chemical species have been investigated by both theoretical and experimental methods. The nature of the chemical bonding in H_3^+ has been studied by means of a natural spin orbital analysis of a previously calculated wavefunction. H_3^+ is shown to resemble closely its united atom analog, Li^+, and the Hartree-Fock energy of H_3^+ is estimated to be -1.301 hartrees. Also, electron density plots are presented in order to clarify the physical picture of the bonding in H_3^+, and suggestions are made as to how further calculations might proceed most efficiently. In the geminal theory of chemical bonding a new method has been developed for solving the coupled integro-differential equations for determination of the optical geminals for a system. Geminal theory has also been generalized to include odd electron systems. A microwave spectrometer employing Zeeman modulation and a flow cell has been built for studying transient paramagnetic species. Charge storage in γ-irradiated polymethylmethacrylate (PMMA) at room temperature has been studied by measuring thermoelectric currents. By using pure PMMA as well as PMMA doped with hole and electron traps it has been shown that added electron traps but not hole traps lead to charge stabilization. The thermoelectric currents appear to be due to hole mobility. The trapped charge in doped PMMA decays with an activation energy of 0.9 ev. Polyvinyl chloride stabilizes even larger amounts of charge than does doped PMMA.

DD FORM 1 JAN 64 1473

UNCLASSIFIED
Security Classification

Unclassified

Security Classification

14. KEY WORDS	LINK A ROLE	LINK A WT	LINK B ROLE	LINK B WT	LINK C ROLE	LINK C WT
H_3^+ bonding						
Geminal theory						
Microwave spectrometer						
Radiolysis of polymethylmethacrylate						
Radiation-induced charge stabilization						
Thermoelectric currents						

INSTRUCTIONS

1. ORIGINATING ACTIVITY: Enter the name and address of the contractor, subcontractor, grantee, Department of Defense activity or other organization *(corporate author)* issuing the report.

2a. REPORT SECURITY CLASSIFICATION: Enter the overall security classification of the report. Indicate whether "Restricted Data" is included. Marking is to be in accordance with appropriate security regulations.

2b. GROUP: Automatic downgrading is specified in DoD Directive 5200.10 and Armed Forces Industrial Manual. Enter the group number. Also, when applicable, show that optional markings have been used for Group 3 and Group 4 as authorized.

3. REPORT TITLE: Enter the complete report title in all capital letters. Titles in all cases should be unclassified. If a meaningful title cannot be selected without classification, show title classification in all capitals in parenthesis immediately following the title.

4. DESCRIPTIVE NOTES: If appropriate, enter the type of report, e.g., interim, progress, summary, annual, or final. Give the inclusive dates when a specific reporting period is covered.

5. AUTHOR(S): Enter the name(s) of author(s) as shown on or in the report. Enter last name, first name, middle initial. If military, show rank and branch of service. The name of the principal author is an absolute minimum requirement.

6. REPORT DATE: Enter the date of the report as day, month, year; or month, year. If more than one date appears on the report, use date of publication.

7a. TOTAL NUMBER OF PAGES: The total page count should follow normal pagination procedures, i.e., enter the number of pages containing information.

7b. NUMBER OF REFERENCES: Enter the total number of references cited in the report.

8a. CONTRACT OR GRANT NUMBER: If appropriate, enter the applicable number of the contract or grant under which the report was written.

8b, 8c, & 8d. PROJECT NUMBER: Enter the appropriate military department identification, such as project number, subproject number, system numbers, task number, etc.

9a. ORIGINATOR'S REPORT NUMBER(S): Enter the official report number by which the document will be identified and controlled by the originating activity. This number must be unique to this report.

9b. OTHER REPORT NUMBER(S): If the report has been assigned any other report numbers *(either by the originator or by the sponsor)*, also enter this number(s).

10. AVAILABILITY/LIMITATION NOTICES: Enter any limitations on further dissemination of the report, other than those imposed by security classification, using standard statements such as:

(1) "Qualified requesters may obtain copies of this report from DDC."

(2) "Foreign announcement and dissemination of this report by DDC is not authorized."

(3) "U. S. Government agencies may obtain copies of this report directly from DDC. Other qualified DDC users shall request through _____."

(4) "U. S. military agencies may obtain copies of this report directly from DDC. Other qualified users shall request through _____."

(5) "All distribution of this report is controlled. Qualified DDC users shall request through _____."

If the report has been furnished to the Office of Technical Services, Department of Commerce, for sale to the public, indicate this fact and enter the price, if known.

11. SUPPLEMENTARY NOTES: Use for additional explanatory notes.

12. SPONSORING MILITARY ACTIVITY: Enter the name of the departmental project office or laboratory sponsoring *(paying for)* the research and development. Include address.

13. ABSTRACT: Enter an abstract giving a brief and factual summary of the document indicative of the report, even though it may also appear elsewhere in the body of the technical report. If additional space is required, a continuation sheet shall be attached.

It is highly desirable that the abstract of classified reports be unclassified. Each paragraph of the abstract shall end with an indication of the military security classification of the information in the paragraph, represented as *(TS)*, *(S)*, *(C)*, or *(U)*.

There is no limitation on the length of the abstract. However, the suggested length is from 150 to 225 words.

14. KEY WORDS: Key words are technically meaningful terms or short phrases that characterize a report and may be used as index entries for cataloging the report. Key words must be selected so that no security classification is required. Identifiers, such as equipment model designation, trade name, military project code name, geographic location, may be used as key words but will be followed by an indication of technical context. The assignment of links, rules, and weights is optional.

Unclassified

Security Classification